Data, Innovation, and Science Cluster Validation Report
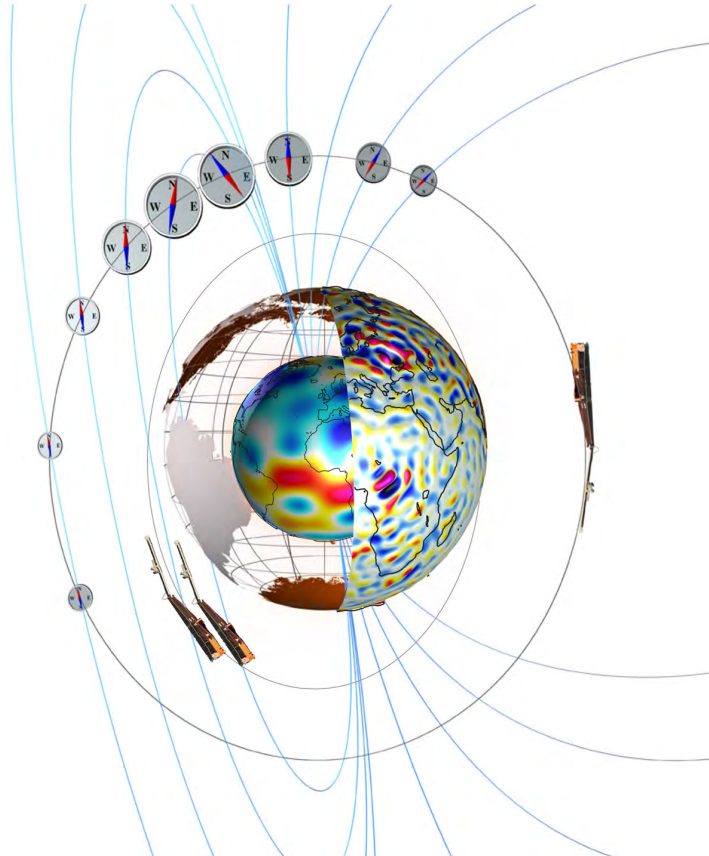
Doc.No: SW-DD-BCSS-GS-0001, Rev: 1

Prepared:

_____
Magnus Danel Hammer   Date 09–06–2020
Scientist

Prepared:

_____
                                       Date 09–06–2020

Approved:

_____
Poul Erik Holmdahl Olsen   Date 09–06–2020
Project Manager

Checked:

_____
Christopher Finlay   Date 09–06–2020
Project Lead

Record of changes

Reason	Description	Rev	Date
Issue 1	First Issue	1	09–06–2020

Table of Contents

Preface

This document reports on the validation of the Swarm DISC Geomagnetic Virtual Observatory (GVO) product files. The GVO product files are described in detail in the Description of Processing Algorithms report, Doc. No. SW-DS-DTU-GS-005.

1 Introduction

1.1 Overview of GVO products

The Swarm DISC GVO product files contain time series of the spherical polar components of the vector geomagnetic field provided on a grid of 300 globally distributed geomagnetic virtual observatories. The GVO time series are derived from magnetic field measurements provided by the three *Swarm* satellites; for details on the data selection and processing, and the GVO computation method see Description of Processing Algorithms report, Doc. No. SW-DS-DTU-GS-005. Two GVO data products are provided:

1. **VOBS_1M_2**: one-monthly GVO time series of the vector magnetic field: the Observed Field, the Core Field and the Secular Variation, and their associated error estimates, all provided on a global grid of geomagnetic virtual observatories

2. **VOBS_4M_2**: four-monthly GVO time series of the vector magnetic field: the Observed Field, the Core Field and the Secular Variation, and their associated error estimates, all provided on a global grid of geomagnetic virtual observatories

This document is concerned with the validation of these GVO data products. The Swarm Level 1b (L1b) MAGX_LR_1B data taken from December 2013 to March 2020 have been used to derive the GVOs used for validation tests presented in this document. The following GVO data product versions were used in this document

- SW_OPER_VOBS_1M_2__20131215T000000_20200315T000000_0101.cdf

- SW_OPER_VOBS_4M_2__20140301T000000_20200301T000000_0101.cdf

To illustrate the Swarm DISC GVO one-monthly data products **VOBS_1M_2**, Figures 1-3 present global maps of annual differences of the spherical polar vector field components of the one-monthly Observed Field GVO time series (blue dots) and of the one-monthly Core field GVO time series (red dots). Figures 4-6 present a similar summary of the global results for the four-monthly products **VOBS_4M_2**.
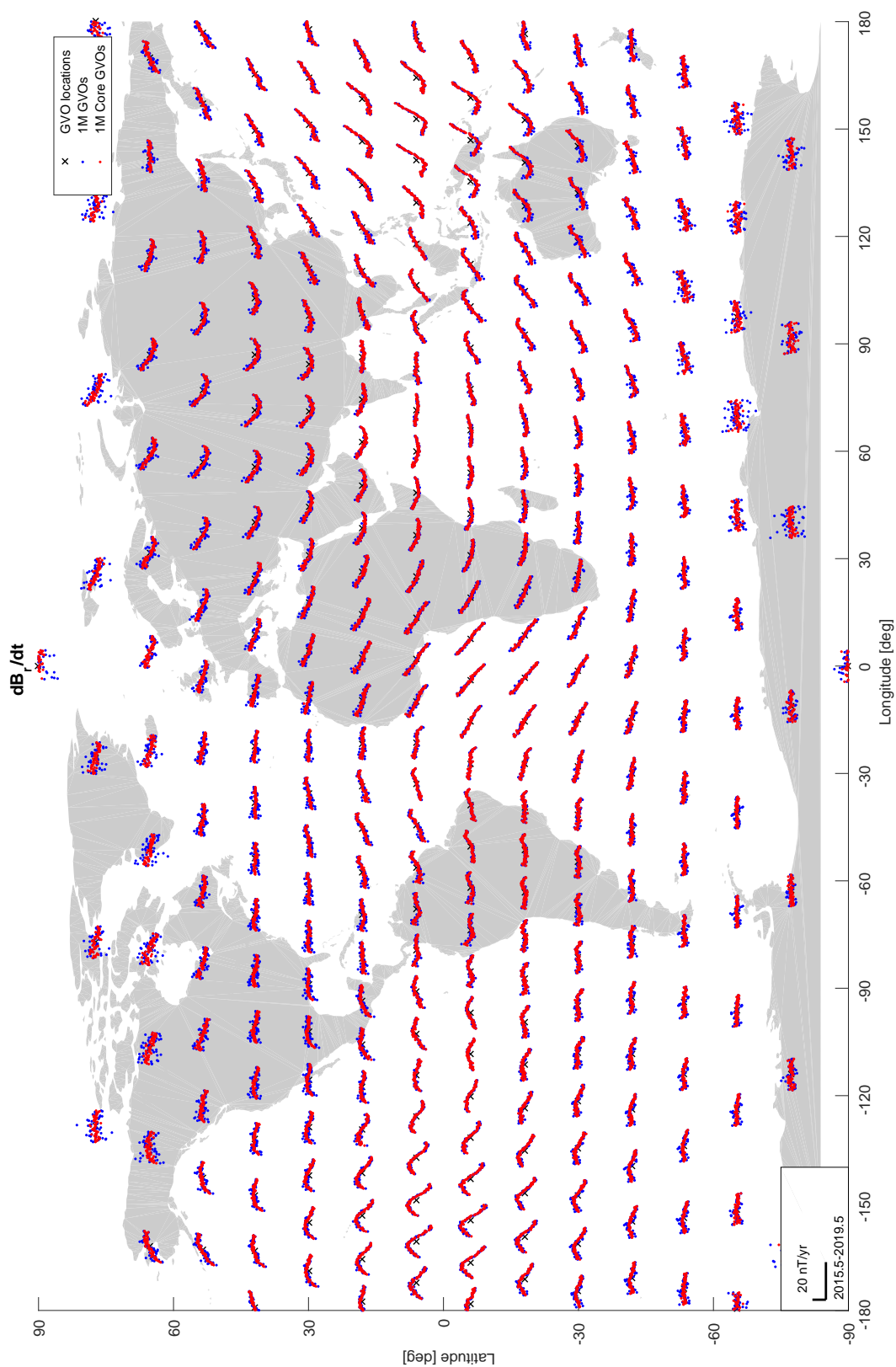
Figure 1: Time series of annual differences of one-monthly GVOs, the Observed Field (blue dots) and the Core Field (red dots). Shown here is the radial r-component. GVO locations are marked with a black cross.
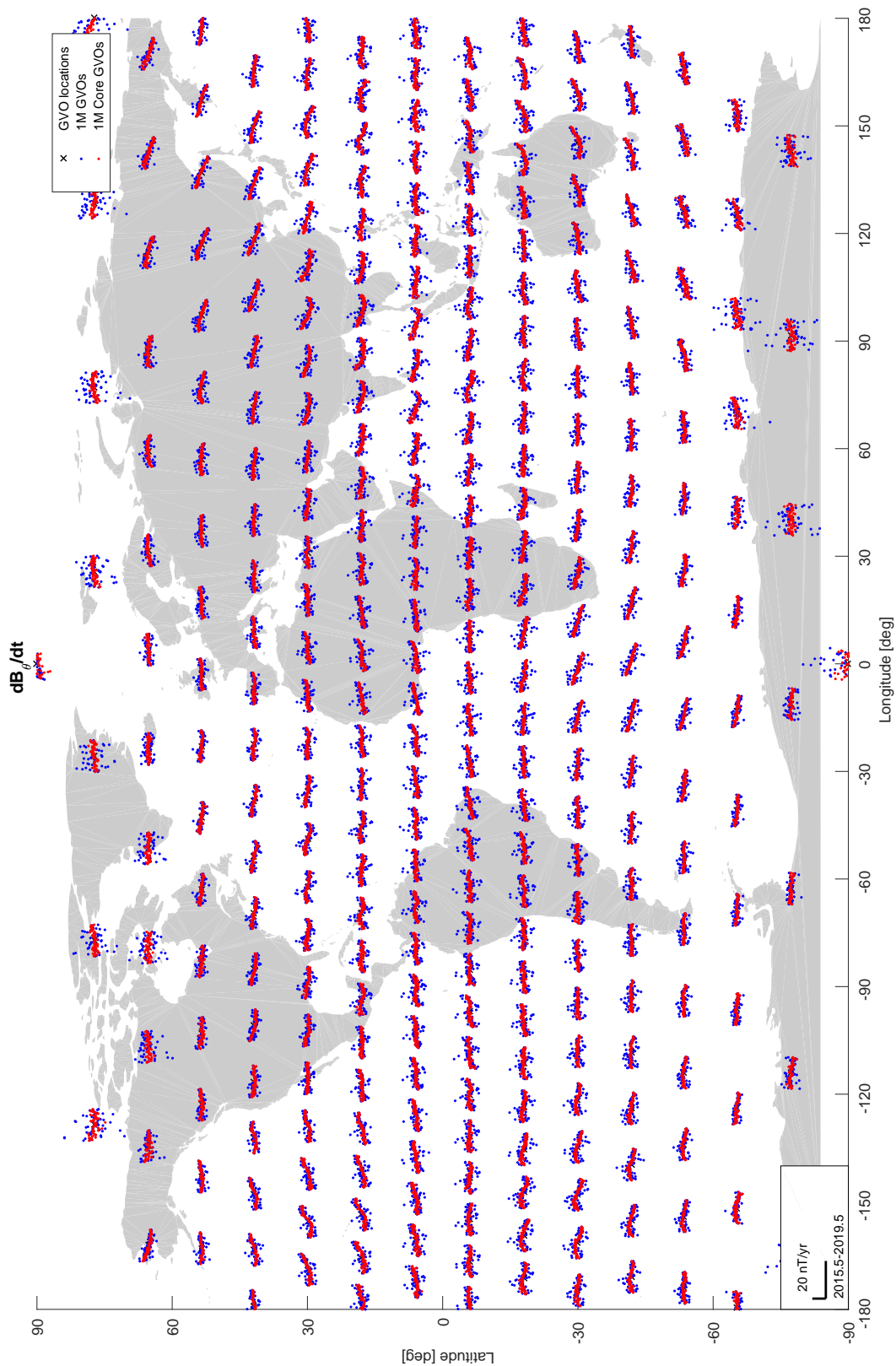
Figure 2: Time series of annual differences of one-monthly GVOs, the Observed Field (blue dots) and the Core Field (red dots). Shown here is the southward θ-component. GVO locations are marked with a black cross.
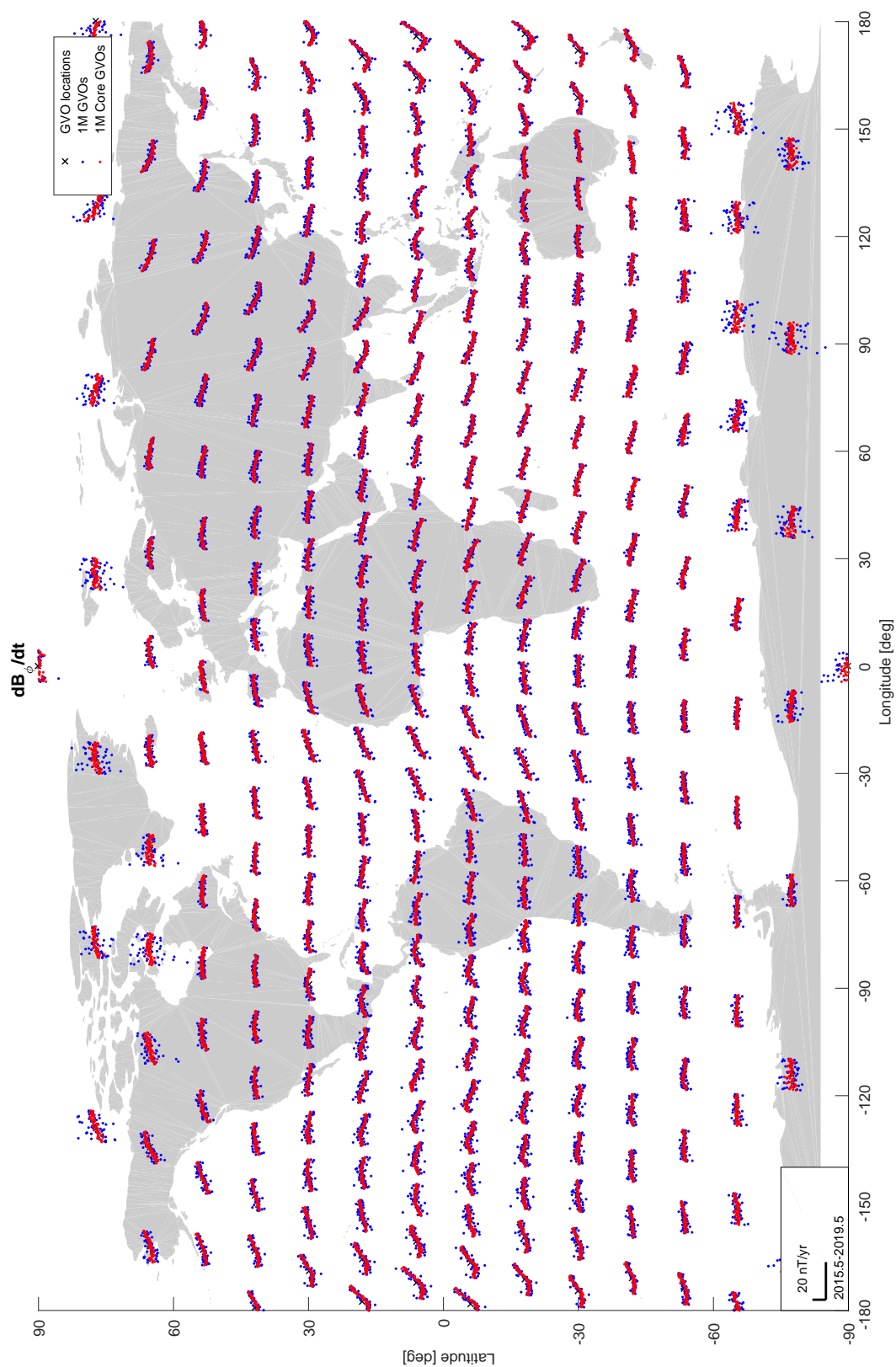
Figure 3: Time series of annual differences of one-monthly GVOs, the Observed Field (blue dots) and the Core Field (red dots). Shown here is the eastward ϕ-component. GVO locations are marked with a black cross.
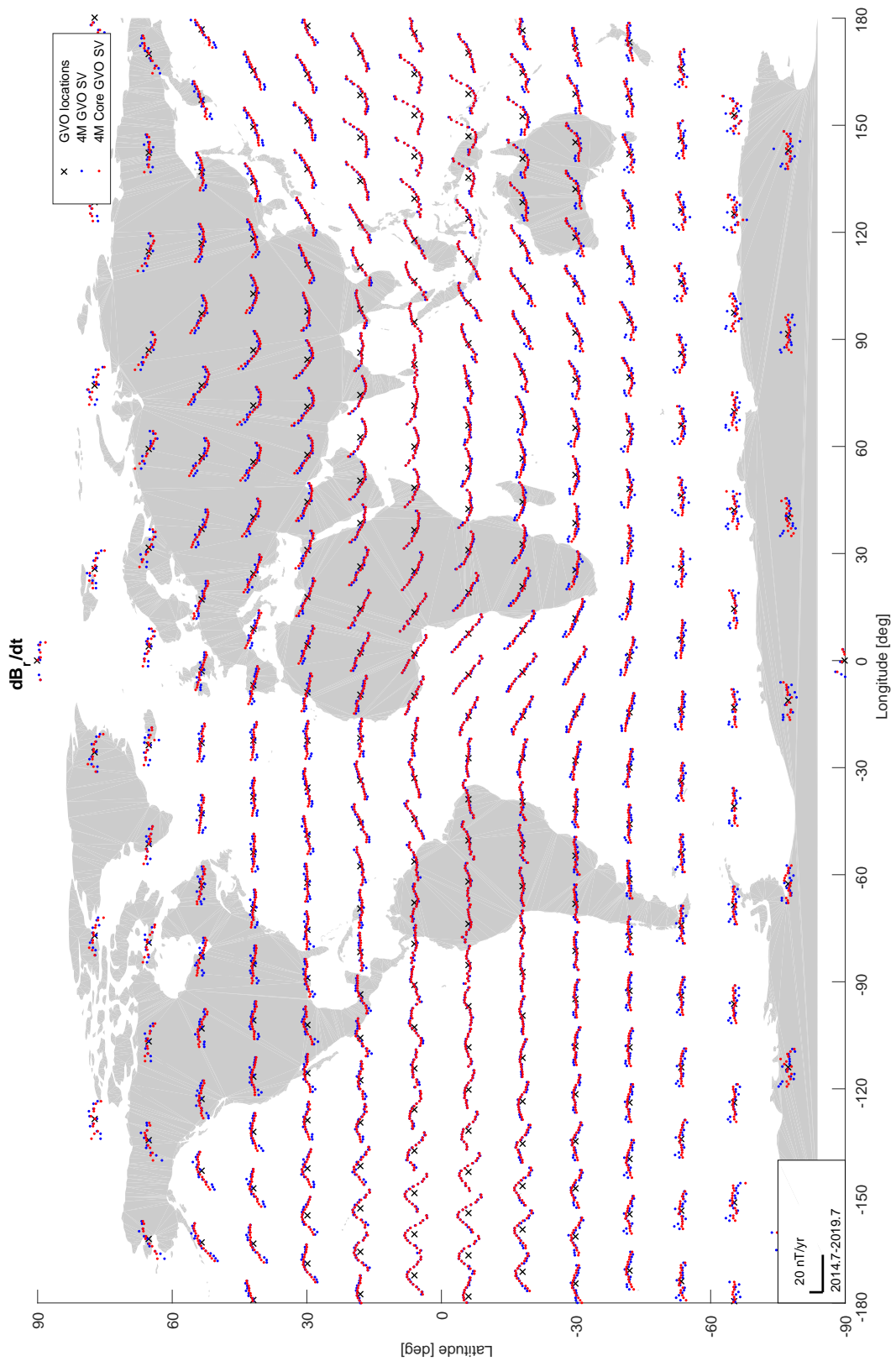
Figure 4: Time series of annual differences of four-monthly GVOs, the Observed Field (blue dots) and the Core Field (red dots). Shown here is the radial r-component. GVO locations are marked with a black cross.
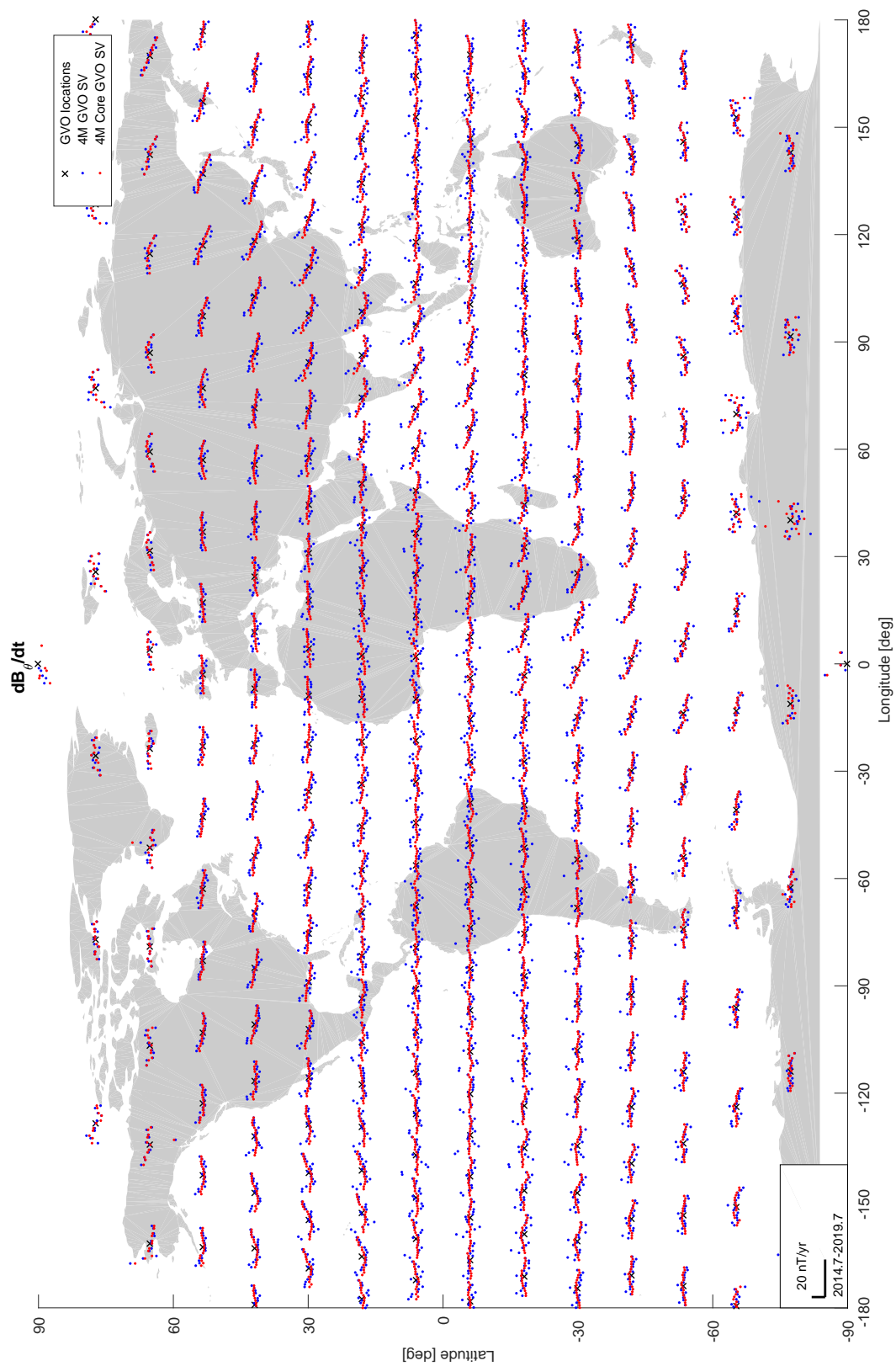
Figure 5: Time series of annual differences of four-monthly GVOs, the Observed Field (blue dots) and the Core Field (red dots). Shown here is the southward θ-component. GVO locations are marked with a black cross.
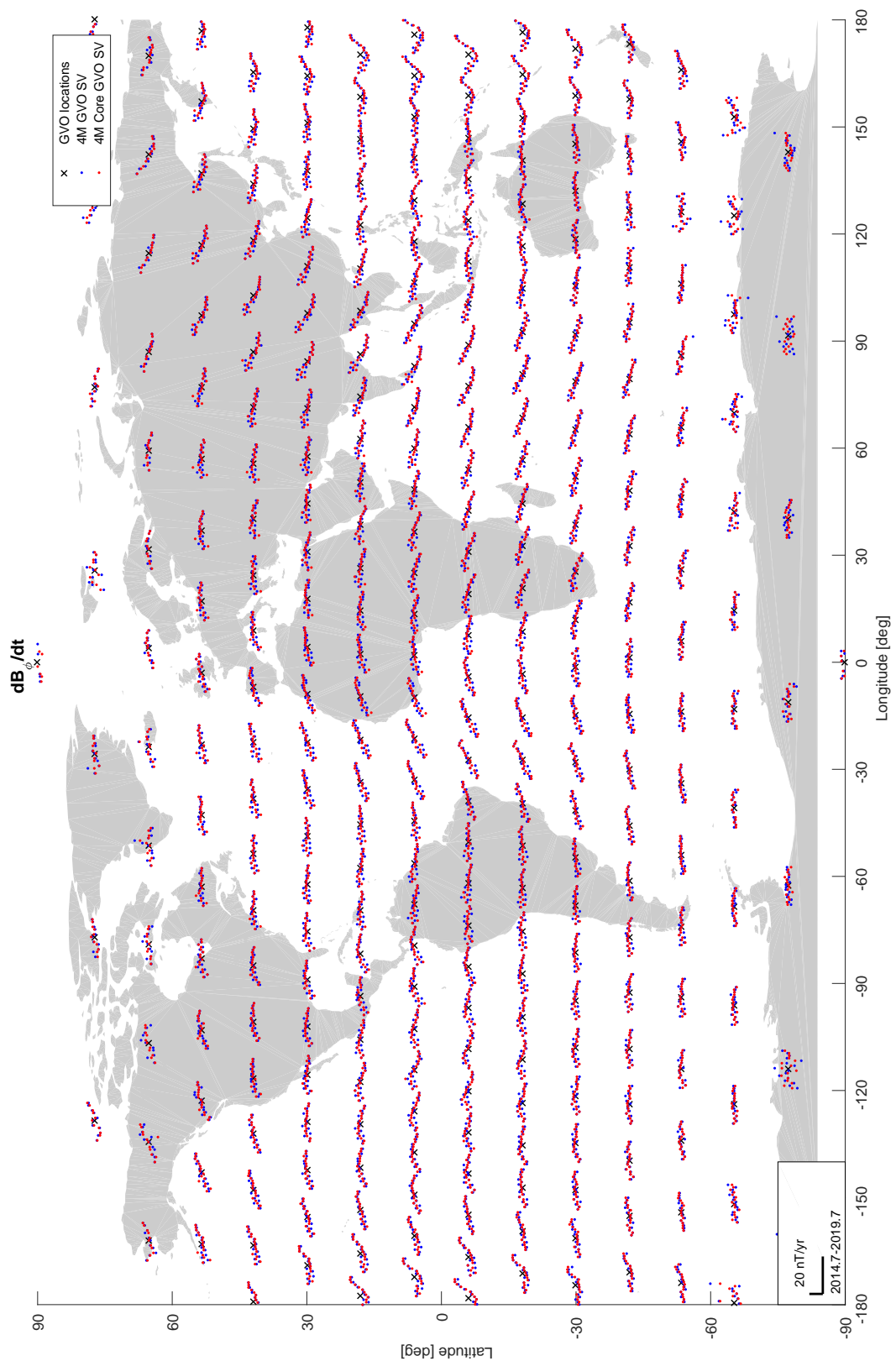
Figure 6: Time series of annual differences of four-monthly GVOs, the Observed Field (blue dots) and the Core Field (red dots). Shown here is the eastward ϕ-component. GVO locations are marked with a black cross.

1.2   Tests against independent ground magnetic observatory data

The first validation tests carried out were comparisons between the GVO products and independent ground observatory (GObs) records, which are the established standard reference data series for monitoring long-term variations in the geomagnetic field.

In our tests we considered data from 28 INTERMAGNET (International Real-time Magnetic Observatory Network) ground observatories, listed in Table 1 and shown as the blue dots in Figure 7. These were chosen for their representative geographic coverage, spanning both polar and non-polar latitudes and all longitude sectors. Below we refer to polar stations as being the 13 stations with colatitudes 0° to 36° and 144° to 180°, with the remaining 15 stations referred to as non-polar stations. From these stations we further selected six 'benchmark' stations (Chambon la Forêt, Kakioka, Honolulu, Guam, Hermanus and Canberra) from mid-to-low latitudes that are well known for their high quality. We use these in an attempt to establish, under well-understood conditions, the extent to which *Swarm* GVO series agree with ground records, with an emphasis on how well the core field secular variation is captured.
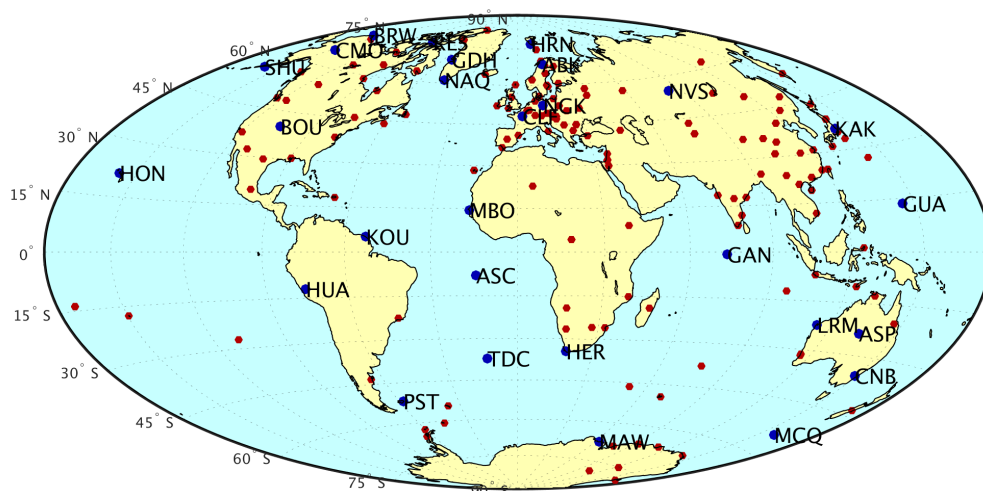
Figure 7: Ground observatories selected for validation tests of the GVO series (blue symbols), other ground observatories marked by red symbols.

We use the Swarm AUX_OBS_2_ hourly mean dataset maintained by BGS, version 0122 from February 2020, retrieved from `ftp://ftp.nerc-murchison.ac.uk/geomag/Swarm/AUX_OBS`. These data have been checked and corrected for known baseline jumps [Macmillan and Olsen, 2013].

From these hourly mean values for each selected observatory we compute:

(i) one-monthly and four-monthly simple mean field values, for each of the three spherical polar components. These are used for comparisons with the Observed Field GVO products.

(ii) revised monthly means [Olsen et al., 2014], wherein the CHAOS magnetospheric field and CM4 ionospheric field predictions (and their induced counterparts) are first removed from the hourly means for each of the three spherical polar components and then robust (Huber-weighted) means are computed over one-monthly and four-monthly time windows. These series are used for comparisons with the Core Field and Secular Variation GVO products.

To enable direct comparisons with these ground observatory series, we computed dedicated GVO time series directly above each selected ground observatory, using the approach described in

Observatory name	IAGA code	Colatitude	East longitude
Abisko	ABK	21.642°	18.823°
Ascension Island	ASC	97.95°	345.62°
Alice Springs	ASP	113.77°	133.88°
Boulder	BOU	49.87°	254.77°
Barrow	BRW	18.68°	203.38°
Chambon la Forêt	CLF	41.98°	2.27°
College	CMO	25.13°	212.14°
Canberra	CNB	125.32°	149.36°
Gan	GAN	89.3054°	73.1537°
Qeqertarsuaq (Godhavn)	GDH	20.748°	306.467°
Guam	GUA	76.41°	144.87°
Hermanus	HER	124.43°	19.23°
Honolulu	HON	68.68°	202.0°
Hornsund	HRN	12.998°	15.547°
Huancayo	HUA	102.05°	284.67°
Kakioka	KAK	53.77°	140.18°
Kourou	KOU	84.79°	307.27°
Learmonth	LRM	112.22°	114.1°
Mawson	MAW	157.6°	62.88°
Mbour	MBO	75.62°	343.03°
Macquarie Island	MCQ	144.5°	158.95°
Narsarsuaq	NAQ	28.84°	314.558°
Niemegk	NGK	37.93°	12.68°
Novosibirsk	NSV	35.15°	83.23°
Port Stanley	PST	141.7°	302.11°
Resolute Bay	RES	15.31°	265.105°
Shumagin	SHU	34.65°	199.54°
Tristan da Cunha	TDC	127.067°	347.685°

Table 1: List of the selected ground observatories used here for validation test, listed in alphabetic order. Source http://www.intermagnet.org/.

the Description of Processing Algorithms report, Section 4.1. We removed crustal bias estimates from each series (computed as the median residual from the CHAOS-7.2 internal field model to up spherical harmonic degree 16) and mapped the GVO estimates downwards to the position of the ground observatory at Earth's surface by removing the difference between the CHAOS-7.2 model predictions at the GVO location and at the ground observatory location, resulting in the series $\widetilde{B}_j^{Gobs}(t_i)$ for the ground observatories and $\widetilde{B}_j^{GVO}(t_i)$ for the GVOs respectively, each at the ground observatory location where the subscript j indicates either the r, θ or ϕ component, or the scalar field intensity F (the latter was computed by taking the root-sum-square of the three spherical polar components $\widetilde{B}_j^{GVO}(t_i)$ and $\widetilde{B}_j^{Gobs}(t_i)$).

The root-mean-square (rms) deviation between these series was computed as follows

$$\text{rms}_j^{obs} = \sqrt{\frac{1}{N_d} \sum_{i=1}^{N_d} \left[\widetilde{B}_j^{Gobs}(t_i) - \widetilde{B}_j^{GVO}(t_i) \right]^2} \qquad (1)$$

where the summation runs over the length of the time series $i = 1, ..., N_d$. rms differences for secular variation series are computed in the same fashion, using annual differences of $\widetilde{B}_j^{Gobs}(t_i)$ and $\widetilde{B}_j^{GVO}(t_i)$ for the Core Field GVOs respectively. We also compute means over these rms values for groups of series from the polar regions, the non-polar region and benchmark observatories. We used the interval 2015-2018 when there is good availability of definitive observatory data.

We note that despite being the best available information concerning secular variation, the ground observatory records are themselves inherently imperfect. Membership of INTERMAGNET requires that the accuracy of series be less than 5 nT, with the best observatories having an estimated baseline certainty of up to 0.4 nT [Lesur et al., 2017]. Beyond observatory measurement

uncertainties, a further source of differences between ground observatory data and GVO estimates is that the latter use data above the ionospheric E-layer, while ground data is collected at the Earth's surface. They therefore see ionospheric and magnetosphere-ionosphere coupling currents differently. The potential field mapping used to downward continue GVOs to Earth's surface does not account for this difference, so it is a source of discrepancy between the two series, particularly in the horizontal components.

1.3 Tests against field model predictions

The second set of tests carried out involved comparisons between the GVO products and predictions from geomagnetic field models. These have the advantage that the GVO product global grids can be tested directly and the global validity of the products can be assessed. However, unlike the comparisons with ground observatories, tests against field model predictions are not fully independent as *Swarm* data were also used in the construction of the field models.

Comparisons to models are based on the root-mean-square (rms) deviation between a given GVO time series $B_j^{GVO}(t_i)$ and field model predictions at the same location and times $B_j^{mod}(t_i)$,

$$\text{rms}_j^{mod} = \sqrt{\frac{1}{N_d} \sum_{i=1}^{N_d} \left[B_j^{mod}(t_i) - B_j^{GVO}(t_i) \right]^2} \tag{2}$$

where the summation runs over the length of the time series $i = 1, ..., N_d$ and j indicates a specific spherical polar component r, θ, ϕ of the vector field or F for scalar field intensity, which is computed from the root-mean-square of the three spherical polar components.

For comparisons with the Core Field GVOs $B_j^{mod}(t_i)$ is computed using the time-dependent internal field from the CHAOS-7.2 model [Finlay et al., 2020] for spherical harmonic degrees up to 20, with the LCS-1 lithospheric model [Olsen et al., 2017] for degree 14-20 removed. For comparisons with the Core Field Secular Variation GVOs, $B_j^{mod}(t_i)$ is computed using the first time derivative of the time-dependent internal field from CHAOS-7.2. In the global grid there are 78 polar and 222 non-polar GVOs and Benchmark values were computed using GVO locations with latitudes below 30 degrees. Comparisons were made between 2014 and 2020, when GVO data were available.

For comparisons with the Observed Field GVOs, $B_j^{mod}(t_i)$ is computed using the CHAOS-7.2 time-dependent internal field for degrees 1 to 13, the LCS-1 lithopsheric field model degrees 14-185, as well as the CHAOS-7.2 magnetospheric field (and induced counterparts) and the CIY4 ionospheric field [Sabaka et al., 2018] (and induced counterparts). The magnetospheric and ionospheric fields and their counterparts are computed as mean values for each 1-monthly or 4-monthly time window, considering the times of the actual data used to derived the GVO estimates. We note the model values compared to the Observed Field GVOs are not fully representative of all the fields contributing to the GVOs, in particular they do not include realistic ionospheric fields in the polar region, or magnetosphere-ionosphere coupling currents.

1.4 Structure of this document

The validation tests reported in this document are arranged as follows:

- Validation of the one-monthly Observed Field GVOs - Section 2.1

- Validation of the four-monthly Observed Field GVOs - Section 2.2

- Validation of the one-monthly Core Field and Secular Variation GVOs - Section 3.1

- Validation of the four-monthly Core Field and Secular Variation GVOs - Section 3.2

2   Observed Field GVO Time Series

2.1   One-Monthly Observed Field GVOs

The one-monthly Observed Field GVO time series are computed from satellite magnetic field measurements with no data selection criteria applied, no estimates of magnetospheric nor ionospheric fields are removed and no PCA denoising or spherical harmonic analysis is applied.

Table 2 presents the rms differences between the one-monthly Observed Field GVO dataset and the 28 selected ground observatories listed in table 1 computed as described by equation (1) for each spherical polar field component as well as the scalar field intensity. For the 28 selected stations the average rms values are 3.00 nT, 6.98 nT, 5.25 nT for the radial, θ and ϕ components, respectively. The differences at stations in the polar regions, where ionospheric currents have a strong signature, are higher, particularly for the horizontal field components. At the six selected mid and low latitude benchmark stations the mean rms differences are 1.67 nT, 3.71 nT and 3.32 nT respectively for the radial, θ and ϕ components.

Observatory	rms_r^{obs} [nT]	$\mathrm{rms}_\theta^{obs}$ [nT]	rms_ϕ^{obs} [nT]	rms_F^{obs} [nT]
ABK	3.01	8.18	4.18	3.50
ASC	1.29	3.26	4.10	2.44
ASP	1.75	4.16	2.48	2.45
BOU	2.52	4.10	2.37	2.78
BRW	7.13	20.04	7.25	7.73
CLF	2.06	3.21	3.22	2.03
CMO	3.73	8.73	6.17	4.80
CNB	1.25	3.61	2.20	1.66
GAN	1.25	3.76	2.56	3.51
GDH	6.33	13.30	19.12	6.74
GUA	2.17	3.68	3.53	3.82
HER	1.35	4.13	3.37	2.20
HON	1.66	3.94	4.09	3.37
HRN	6.01	20.69	16.37	7.04
HUA	7.13	20.04	7.25	7.73
KAK	1.50	3.69	3.49	2.08
KOU	3.18	4.07	3.87	3.45
LRM	2.41	3.43	3.53	2.86
MAW	6.97	15.74	11.35	8.47
MBO	2.46	6.46	4.27	2.63
MCQ	2.76	4.52	3.89	4.55
NAQ	4.31	8.55	5.03	4.11
NGK	2.18	3.61	3.03	2.07
NSV	2.08	4.09	3.02	2.05
PST	1.85	6.19	3.42	3.76
RES	7.28	13.59	8.94	7.23
SHU	2.24	4.75	2.32	2.69
TDC	1.00	5.01	3.81	2.52
ALL	3.00	6.98	5.25	3.91
Polar	4.28	10.30	7.27	4.83
Non-Polar	1.90	4.11	3.51	3.12
Benchmark	1.67	3.71	3.32	2.53

Table 2: One-monthly Observed Field GVOs versus selected Ground Observatories: rms differences for the spherical polar vector components and field intensity in nT.

More detailed insight comes from directly examining the time series of the Ground Observatory and associated GVO series. Figure 8 presents the Observed Field GVO estimates, mapped down to Earth's surface, compared to one-monthly ground observatory mean values, at five of the benchmark observatories from mid and low latitudes. When examining the Observed Field GVOs we consider time series of the field itself, rather than the secular variation, to directly assess the GVO product so as not to filter out any signals that may be of interest by taking annual differences.
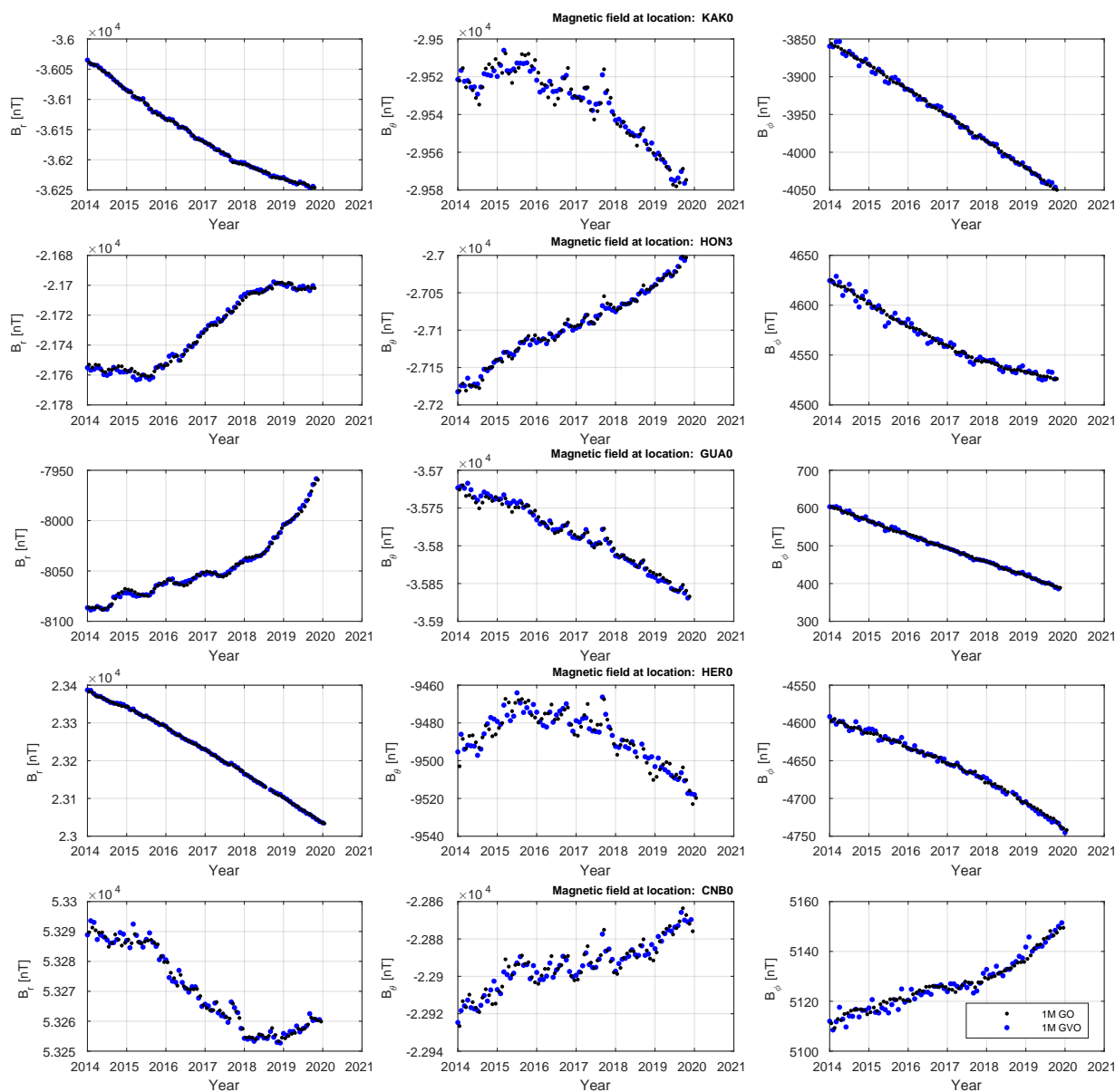
Figure 8: One-monthly Observed Field GVO estimates mapped to Earth's surface (blue symbols) and one-monthly means from selected high quality 'benchmark' ground observatories from mid and low latitude (black symbols), arranged from north to south in the rows. Left column is the radial field component, middle column is the southward field component, right column is the eastward field component, units are nT.

Signals in the radial field in the benchmark stations are followed closely by the GVO series, for example in the series from Kakioka (KAK0), where both the trend in the field and its acceleration are followed, and the rms difference between the series is 1.5 nT. The observed field GVO series are also seen to follow annual signals in the radial field e.g. at Guam (GUA0). The ability of the Observed Field GVO series to track sub-annual field changes is illustrated in the southward θ component series, for example see the peak observed in the second half of 2017. This feature, likely of magnetospheric origin, is seen simultaneously at all benchmark stations in both the GVO

and Gobs series, and is seen particularly clearly at Kakioka (KAK0) and Hermanus (HER0). The amplitude of the peak seems to be slightly lower in the GVO series. More scatter is seen in the eastward ϕ components of the GVO series compared to the ground observatory benchmark series (e.g. at Honolulu, HON3). The source of this scatter may be ionospheric or field aligned currents seen by the satellites that are less prominent on ground; the amplitude of the scatter was larger 2014-2016, which may indicate a solar cycle dependence.
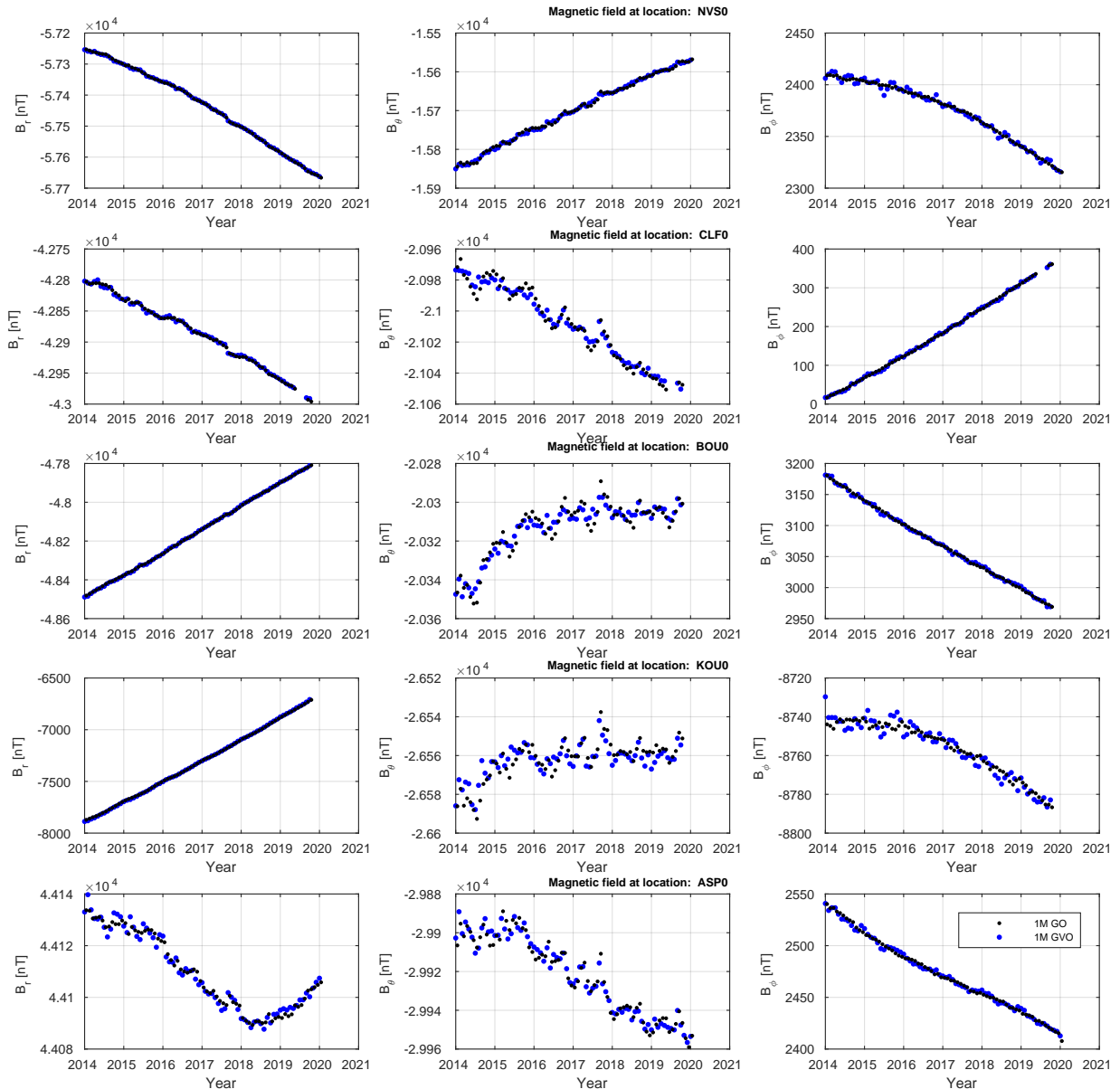
Figure 9: One-monthly Observed Field GVO estimates mapped to Earth's surface (blue symbols) and one-monthly means from selected non-polar ground observatories (black symbols), arranged from north to south in the rows. Left column is the radial field component, middle column is the southward field component, right column is the eastward field component, units are nT.

Further examples of non-polar Ground Observatories and one-monthly Observed Field GVO estimates are presented in Figure 9, where similar patterns are seen. Note that the local-time of

the satellites will also play a role for these one-monthly Observed Field GVOs.

Figure 10 presents Observed Field GVO estimates and ground observatory one-monthly means from stations in the polar regions. In these locations, there are strong ionospheric currents between the satellites and the ground stations, and the satellites are flying through strong field-aligned currents. Nonetheless, the comparisons are encouraging and the trends seen at the ground stations are well captured by the GVO series.
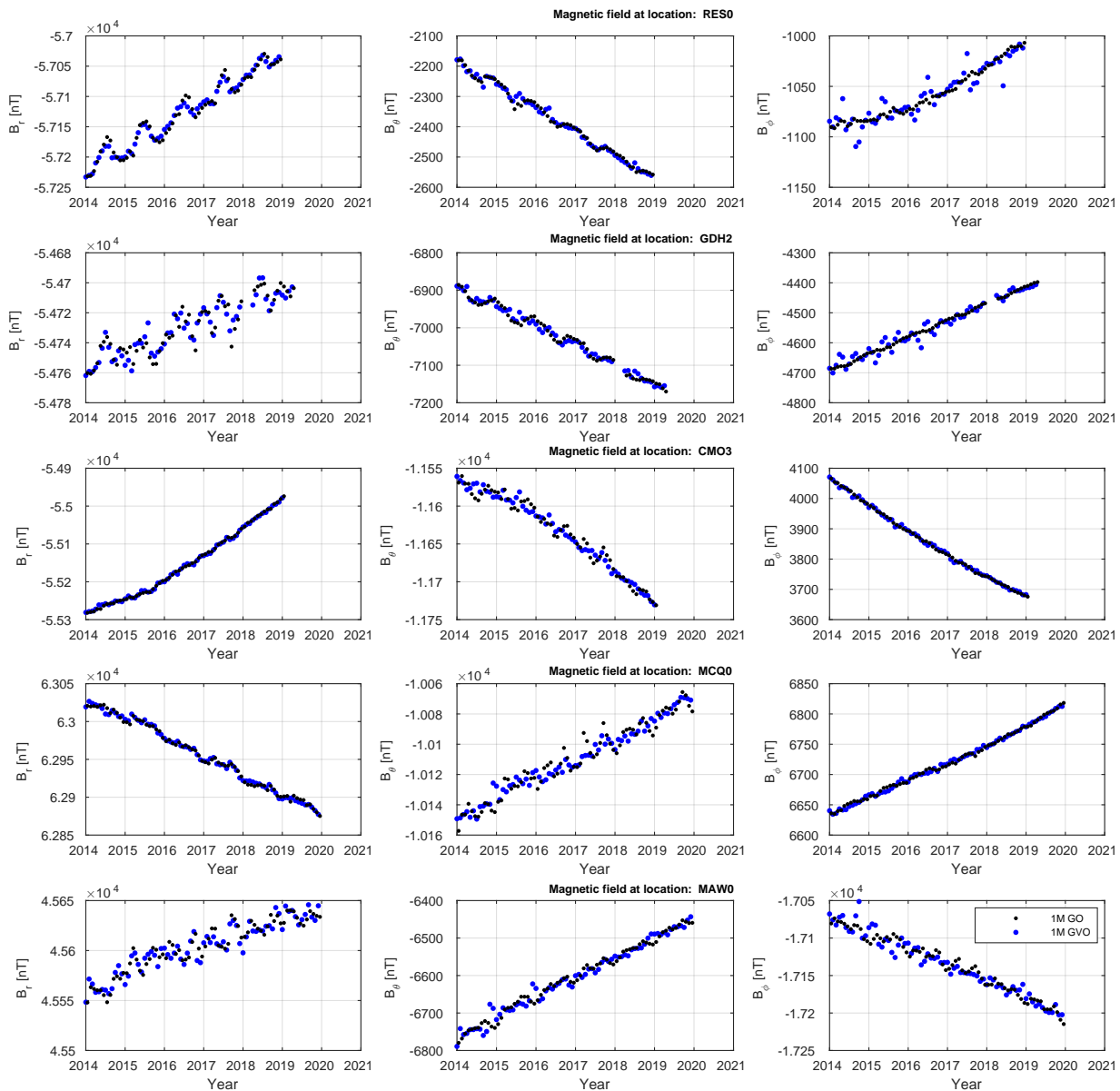
Figure 10: One-monthly Observed Field GVO estimates mapped to Earth's surface (blue symbols) and one-monthly means from selected polar ground observatories (black symbols), arranged from north to south in the rows. Left column is the radial field component, middle column is the southward field component, right column is the eastward field component, units are nT.

The radial component at high northern latitudes in Canada, at the Resolute Bay observatory (RES0) inside the polar cap, shows a particularly clear annual variation in the monthly means,

peaking in the northern summer. These fluctuations, which are likely due to far-field effects of ionospheric currents, are well tracked by the GVO estimates. Seasonal variations in the radial component close to the cusp region, measured on the ground at Qeqertarsuaq (GDH2), are also in the GVO estimates, albeit with some scatter. The southward θ series are also well correlated at these stations. Larger differences are seen in the eastward ϕ components in these stations, the difference are largest 2014-2017, with largest differences (of up to 25 nT seen at RES0 in summer months). The eastward ϕ component in the GVO and ground ground stations agrees more closely in the auroral zone in both the northern hemisphere (in Alaska at College station CMO3) and in the Southern hemisphere at Macquarie Island (MCQ0). These ground station see signals in the southward θ components that are less prominent in the GVO estimates; these are may be due to polar electrojet currents that are closer to the ground stations. At Mawson Observatory in Antarctica (MAW0) the southward θ components fluctuations have the opposite sign to fluctuations seen at the same time in the GVO estimates. The relative position and orientations of the ionospheric currents and the ground and satellite reference points are clearly important for understanding such effects.

Figures showing similar comparisons to all the other considered ground observatories are collected in the Appendix.

In Table 3 rms differences between the one-month GVO time series and model predictions are presented, as described by equation (2). For the benchmark region (latitudes below 30 degrees), the Observed Field GVOs match the field model predictions to within 4 nT, the differences in the polar region are slightly larger, up to 5.5 nT rms. The limitations of this comparison should however be borne in mind – our models of the magnetospheric field do not well describe the disturbed conditions that are included in the observed field GVOs, ionospheric field models used are purely climatological and the models used do not include field-aligned currents that will be seen in satellite data.

Model series	rms_r^{mod} [nT]	$\mathrm{rms}_\theta^{mod}$ [nT]	rms_ϕ^{mod} [nT]	rms_F^{mod} [nT]
All	4.16	3.59	4.00	3.83
Polar	5.47	5.24	5.19	5.30
Non-polar	3.70	3.01	3.59	3.31
Benchmark	3.80	3.10	3.66	3.42

Table 3: One-monthly Observed Field GVOs versus field model predictions: rms differences for the spherical polar vector components and field intensity in nT.

2.2 Four-Monthly Observed Field GVOs

The four-month Observed Field GVO time series are computed from satellite magnetic field measurements satisfying dark and geomagnetically quiet data selection criteria (see GVO Description of Product Algorithm document). No estimates of magnetospheric or ionospheric fields were removed. Table 4 presents the rms differences between 4-monthly means computed for the selected ground observatories, and 4-monthly Observed Field GVO series mapped down to Earth's surface.

Compared to the one-monthly GVOs, lower rms differences are found, particularly for the horizontal components. This is expected due to four-month averaging which will reduce local time effects, and due to the dark and quiet-time selection criteria. As for the one-monthly observed field GVOs, differences are larger in the polar region.

Observatory	rms_r^{obs} [nT]	$\mathrm{rms}_\theta^{obs}$ [nT]	rms_ϕ^{obs} [nT]	rms_F^{obs} [nT]
ABK	1.26	2.96	3.83	1.83
ASC	1.06	3.70	2.74	3.06
ASP	1.00	2.54	1.77	1.72
BOU	1.44	1.92	2.47	1.47
BRW	6.44	3.52	2.98	6.40
CLF	1.33	3.29	2.22	1.23
CMO	2.20	6.68	3.92	2.78
CNB	0.49	2.58	2.08	1.11
GAN	0.84	3.23	1.76	2.96
GDH	5.00	2.65	3.93	5.14
GUA	1.34	3.44	2.16	3.40
HER	1.41	1.53	1.29	1.44
HON	1.45	3.60	1.99	3.05
HRN	5.20	3.96	5.47	4.90
HUA	6.44	3.52	2.98	6.40
KAK	1.90	3.09	1.81	1.32
KOU	2.84	3.83	2.96	3.23
LRM	1.44	2.77	1.55	1.53
MAW	6.01	15.01	5.61	6.30
MBO	2.30	4.70	3.47	2.93
MCQ	3.58	4.30	2.55	4.12
NAQ	2.74	5.77	3.70	1.53
NGK	1.54	2.51	2.19	1.08
NSV	1.74	5.05	1.40	1.18
PST	2.08	2.75	1.49	1.77
RES	3.08	0.63	2.68	3.03
SHU	1.45	2.33	2.09	1.08
TDC	0.83	2.68	2.36	1.85
ALL	2.28	3.72	2.69	2.66
Polar	3.16	4.50	3.29	3.07
Non-Polar	1.51	3.04	2.17	2.31
Benchmark	1.32	2.92	1.93	1.93

Table 4: Four-monthly Observed Field GVOs versus selected Ground Observatories: rms differences for the spherical polar vector components and field intensity in nT.

Figures 11 to 13 present comparisons the four-monthly mean ground observatory time series (in black dots) and the associated fourly-month Observed Field GVO estimates mapped to the Earth's surface (in blue dots) for the same stations as considered above for the one-monthly series.

The two time series for the radial field at the benchmark stations agree very well. Departures from the trends are less prominent in the four-monthly series. Points departing from the trends in the southward θ component are often seen independently in both the ground and satellite series, for example at Guam (GUA0) in late 2017 and in the series from Boulder (BOU0) in Figure 12. As in the one-monthly series, these signals are likely to originate in fluctuations of magnetospheric currents such as the ring current.

Turning to the stations in the polar regions in Figure 13 taking four-monthly means significantly
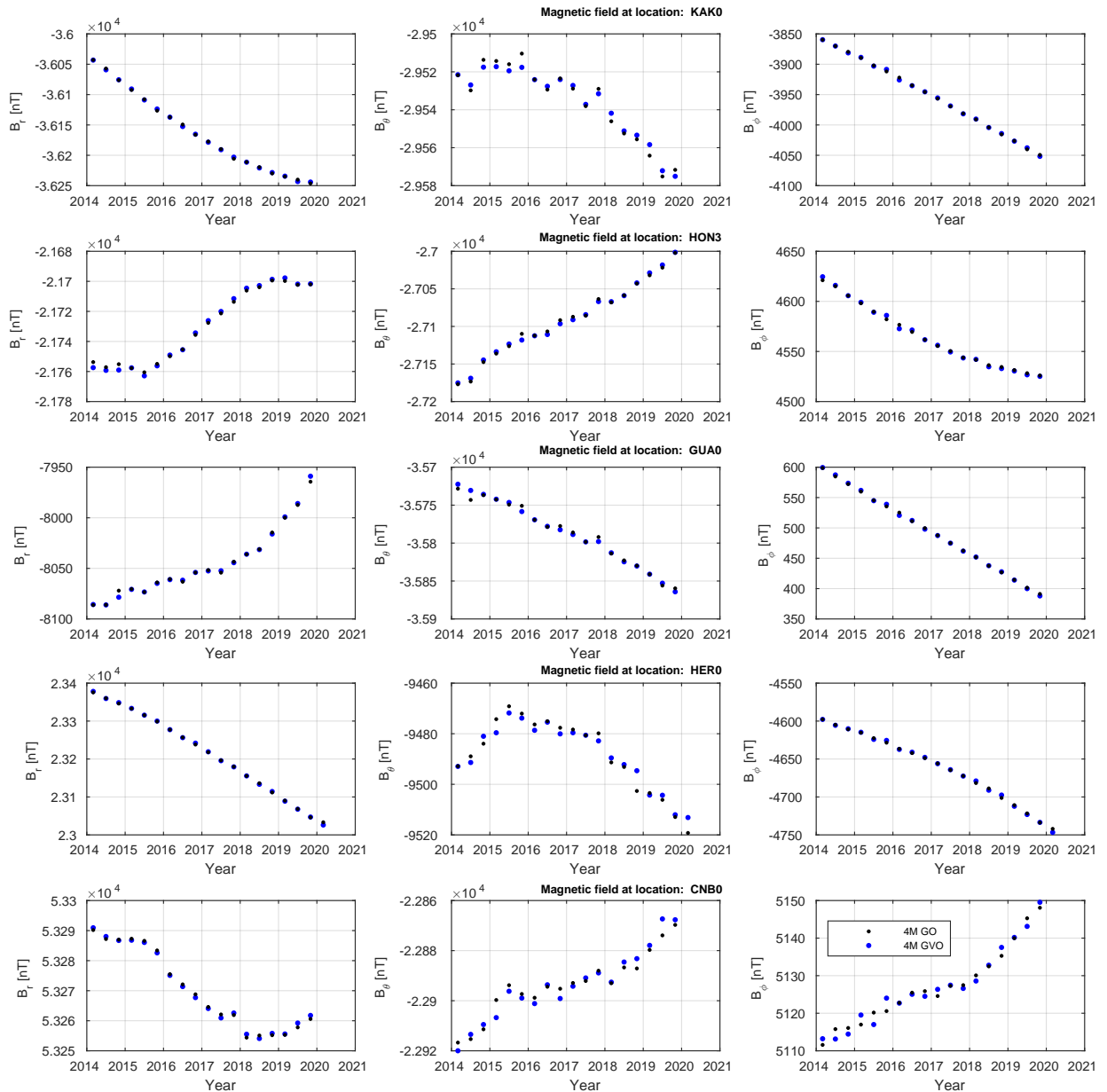
Figure 11: Four-monthly Observed Field GVO estimates mapped to Earth's surface (blue symbols) and four-monthly means from selected high quality 'benchmark' ground observatories from mid and low latitude (black symbols), arranged from north to south in the rows. Left column is the radial field component, middle column is the southward field component, right column is the eastward field component, units are nT.

reduces the scatter. It is clear that the trends seen in the ground stations are well captured by the GVO series. Small additional signals, including annual signals, nonetheless remain in the GVO series, which is to be expected given they use data collected from low Earth-orbit where there are strong field-aligned currents at satellite altitude.

Table 5 presents the rms differences between the four-monthly Observed Field GVOs and model predictions. Compared with the one-monthly statistics in Table 3, the four-monthly Observed Field
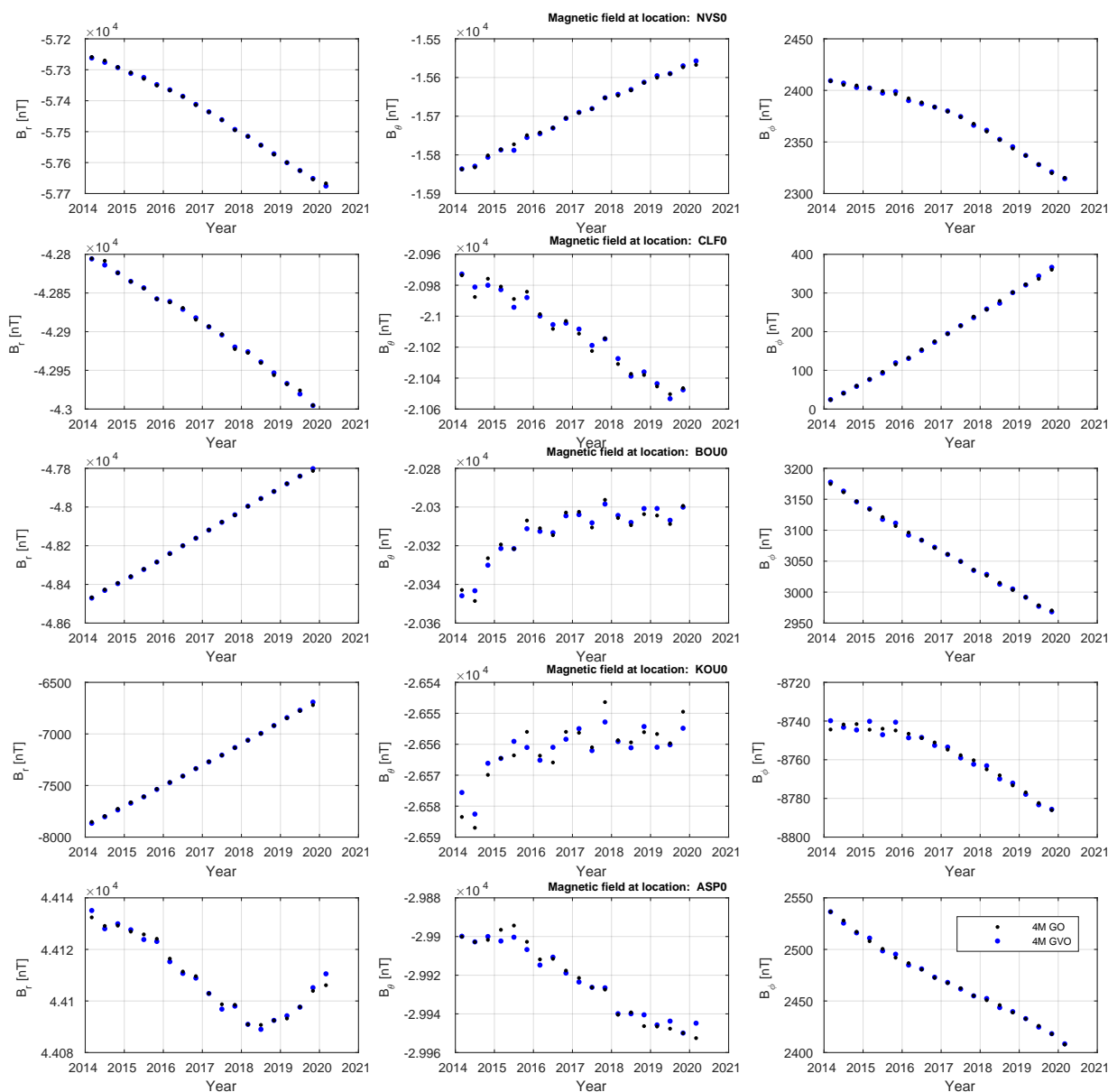
Figure 12: One-monthly Observed Field GVO estimates mapped to Earth's surface (blue symbols) and one-monthly means from selected non-polar ground observatories (black symbols), arranged from north to south in the rows. Left column is the radial field component, middle column is the southward field component, right column is the eastward field component, units are nT.

GVOs agree better with the model predictions. This was expected since the quiet-time selection criteria better match that of the CHAOS magnetospheric field model, and 4-monthly means are more appropriate for comparisons with climatological models of the ionospheric field.
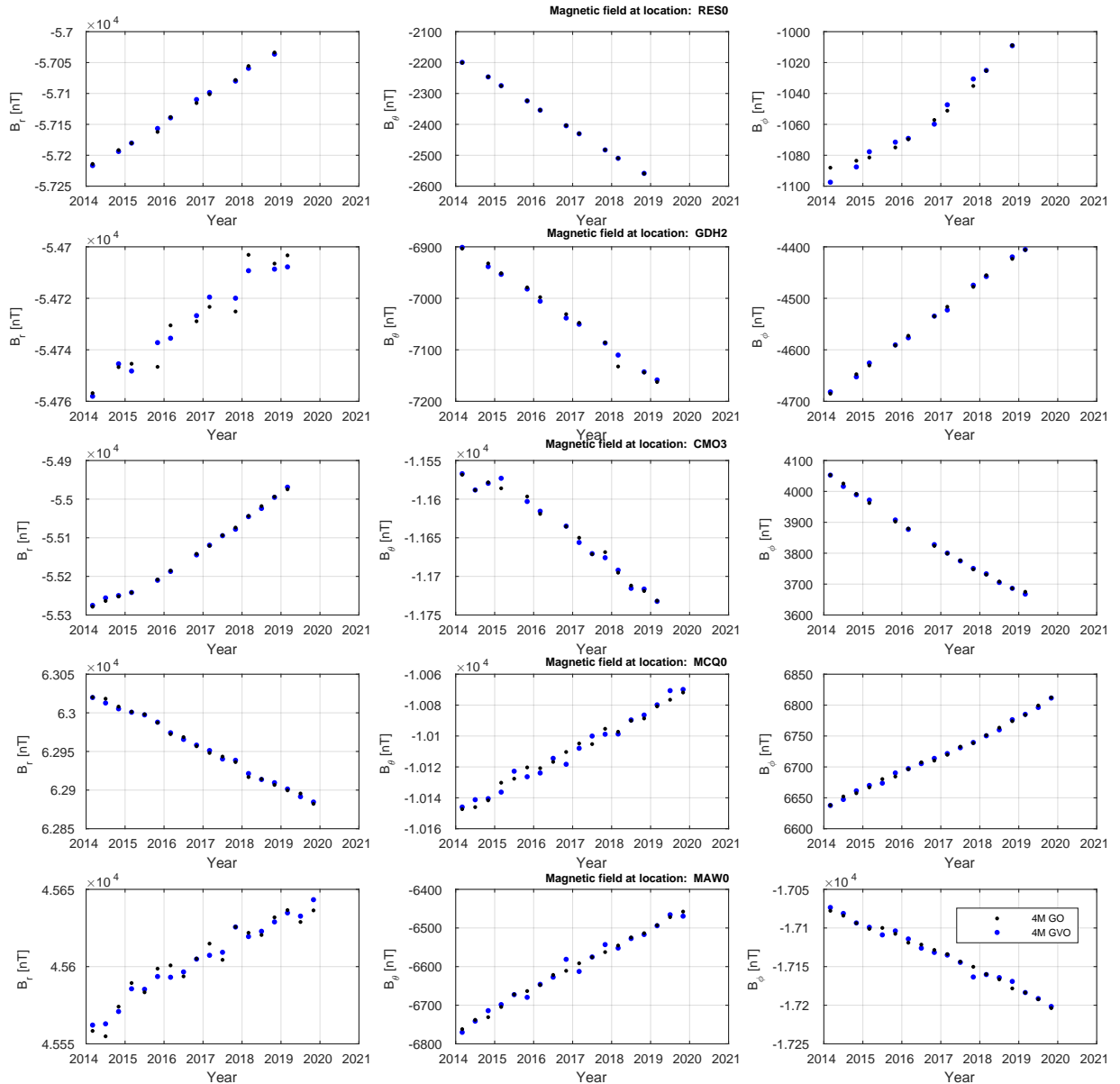
Figure 13: Four-monthly Observed Field GVO estimates mapped to Earth's surface (blue symbols) and four-monthly means from selected polar ground observatories from mid and low latitude (black symbols), arranged from north to south in the rows. Left column is the radial field component, middle column is the southward field component, right column is the eastward field component, units are nT.

Model series	rms$_r^{mod}$ [nT]	rms$_\theta^{mod}$ [nT]	rms$_\phi^{mod}$ [nT]	rms$_F^{mod}$ [nT]
All	2.35	2.66	2.03	2.56
Polar	2.69	3.78	3.27	2.55
Non-polar	2.23	2.26	1.59	2.56
Benchmark	2.26	2.41	1.56	2.74

Table 5: Four-monthly Observed Field GVOs versus field model predictions: rms differences for the spherical polar vector components and field intensity in nT.

3 Core Field and Secular Variation GVO Time Series

3.1 One-Monthly Core Field GVOs and Secular Variation

One-monthly Core Field GVO time series are derived by applying a PCA denoising scheme to the GVO series, and then subtracting estimates of the remaining external and toroidal field obtained using an epoch-by-epoch spherical harmonic analysis (for details see Description of Processing Algorithms document, Sections 4.2 and 4.3).

Table 6 presents the rms differences between one-monthly revised monthly mean Ground Observatory time series (whose processing aims to isolate the core field signal, see Olsen et al. [2014]) at the same 28 selected stations discussed above, along with one-monthly Core Field GVOs constructed at the same colatitude and longitude and mapped down to Earth's surface.

Observatory	rms_r^{obs} [nT]	$\mathrm{rms}_\theta^{obs}$ [nT]	rms_ϕ^{obs} [nT]	rms_F^{obs} [nT]
ABK	3.68	6.43	4.87	3.84
ASC	1.90	1.87	2.56	1.64
ASP	3.48	4.13	1.30	3.85
BOU	4.07	2.14	1.78	3.86
BRW	9.55	14.25	5.43	9.66
CLF	3.69	2.08	2.44	3.49
CMO	4.99	5.58	4.34	5.22
CNB	2.75	3.24	1.98	2.83
GAN	2.47	3.52	1.53	3.73
GDH	7.79	9.84	9.77	8.48
GUA	2.52	2.19	1.80	2.33
HER	2.12	2.46	2.97	2.58
HON	3.11	2.10	2.25	2.46
HRN	7.84	11.98	9.70	7.75
HUA	9.55	14.25	5.43	9.66
KAK	2.69	2.65	1.89	3.10
KOU	5.06	3.41	2.16	3.65
LRM	4.37	3.96	2.24	4.55
MAW	8.29	10.66	7.29	7.30
MBO	3.78	4.43	2.97	4.18
MCQ	3.18	4.43	1.85	4.70
NAQ	5.30	7.44	5.94	5.74
NGK	3.67	2.43	2.31	3.17
NSV	2.03	2.25	1.72	1.98
PST	2.04	3.29	2.26	2.08
RES	8.37	14.92	8.80	8.01
SHU	2.21	2.90	2.93	2.20
TDC	2.27	2.99	1.35	2.69
ALL	4.12	5.17	3.55	4.37
Polar	5.35	7.42	5.26	5.35
Non-Polar	3.05	3.23	2.08	3.52
Benchmark	2.81	2.45	2.22	2.80

Table 6: One-monthly Core Field GVOs versus selected Ground Observatories: rms differences for the spherical polar vector components and field intensity in nT.

The averages rms differences over all stations are 4.12 nT, 5.17 nT and 3.55 nT respectively for the radial, θ and ϕ components. Differences are as before larger in the polar region and also at the Huancayo observatory (HUA), which is located close to the equatorial electrojet. In this section we present time series of the Core Field Secular variation (computed using annual differences), rather than showing the time series for the Core Field itself, these comparisons are discussed further below.

Comparisons of the global grid of Core Field GVOs to predictions from the time-dependent internal field from the CHAOS-7.2 model are presented in Table 7. The predictions match best, to within 2.2 nT, for the eastward ϕ field component at mid-to-low latitudes. The benchmark comparisons here to model predictions involved GVO estimates at all latitudes below 30 degrees.

Model series	rms$_r$ [nT]	rms$_\theta$ [nT]	rms$_\phi$ [nT]	rms$_F$ [nT]
All	3.84	2.83	2.16	3.67
Polar	4.25	3.51	2.92	4.25
Non-polar	3.69	2.59	1.89	3.46
Benchmark	3.80	2.75	1.89	3.58

Table 7: One-monthly Core Field GVOs versus field model predictions: rms differences for the spherical polar vector components and field intensity in nT.

Perhaps even more interesting than the Core Field itself is the quality of the Core Field Secular Variation, obtained by taking annual differences of the Core Field GVO estimates. Table 8 presents the rms differences between the one-monthly Ground Observatory Core Field SV time series and the associated one-monthly GVO Core Field SV time series, mapped to the ground observatory location. The average rms differences with non-polar ground observatories are 1.86 nT/yr, 2.83 nT/yr, 2.35 nT/yr for the radial, θ and ϕ components, respectively. As before, differences are larger for polar stations but still below 6.2 nT/yr in all three components. Considering the six benchmark observatories at mid-to-low latitudes, the secular variation of the field intensity seen at ground observatories is matched to 1.75 nT/yr by the one-monthly Core Field Secular Variation series.

Observatory	rms$_r$ [nT/yr]	rms$_\theta$ [nT/yr]	rms$_\phi$ [nT/yr]	rms$_F$ [nT/yr]
ABK	3.62	5.14	6.04	3.56
ASC	1.84	2.22	3.96	1.33
ASP	1.11	3.05	1.48	1.78
BOU	1.56	2.27	1.97	1.71
BRW	6.39	8.10	6.26	6.54
CLF	2.28	2.75	2.62	1.70
CMO	3.47	4.33	4.35	3.42
CNB	1.43	2.81	1.97	1.60
GAN	1.34	3.14	1.53	2.90
GDH	6.53	9.42	9.22	6.70
GUA	2.87	1.92	2.39	1.73
HER	1.27	2.08	2.86	1.38
HON	1.40	2.28	2.59	1.92
HRN	7.08	8.23	8.45	6.47
HUA	6.39	8.10	6.26	6.54
KAK	1.54	3.17	1.70	2.15
KOU	3.53	3.56	1.87	2.88
LRM	1.66	2.58	3.29	1.97
MAW	7.45	8.88	6.73	6.81
MBO	3.59	4.49	3.42	3.37
MCQ	1.92	3.84	2.00	3.56
NAQ	3.07	7.02	4.08	3.06
NGK	2.10	3.21	2.51	1.39
NSV	1.92	2.92	1.31	1.68
PST	2.52	3.47	2.51	1.97
RES	8.54	11.88	8.70	8.57
SHU	1.64	2.31	1.87	1.65
TDC	1.70	2.05	1.69	2.49
ALL	3.06	4.35	3.60	3.18
Polar	4.46	6.11	5.03	4.25
Non-Polar	1.86	2.83	2.35	2.26
Benchmark	1.80	2.50	2.35	1.75

Table 8: One-monthly Core Field GVO Secular Variation versus selected Ground Observatories: rms differences for the spherical polar vector components and field intensity in nT/yr.

Figures 14-16 present plots of the one-monthly revised monthly mean SV at example ground stations (black dots) and the one-monthly Core Field GVO SV series (red dots). Figure 14 presents the series at five of the mid and low latitude benchmark locations. Note the difference in scale here

when looking at the secular variation, compared to the earlier plots showing the Observed Field values.
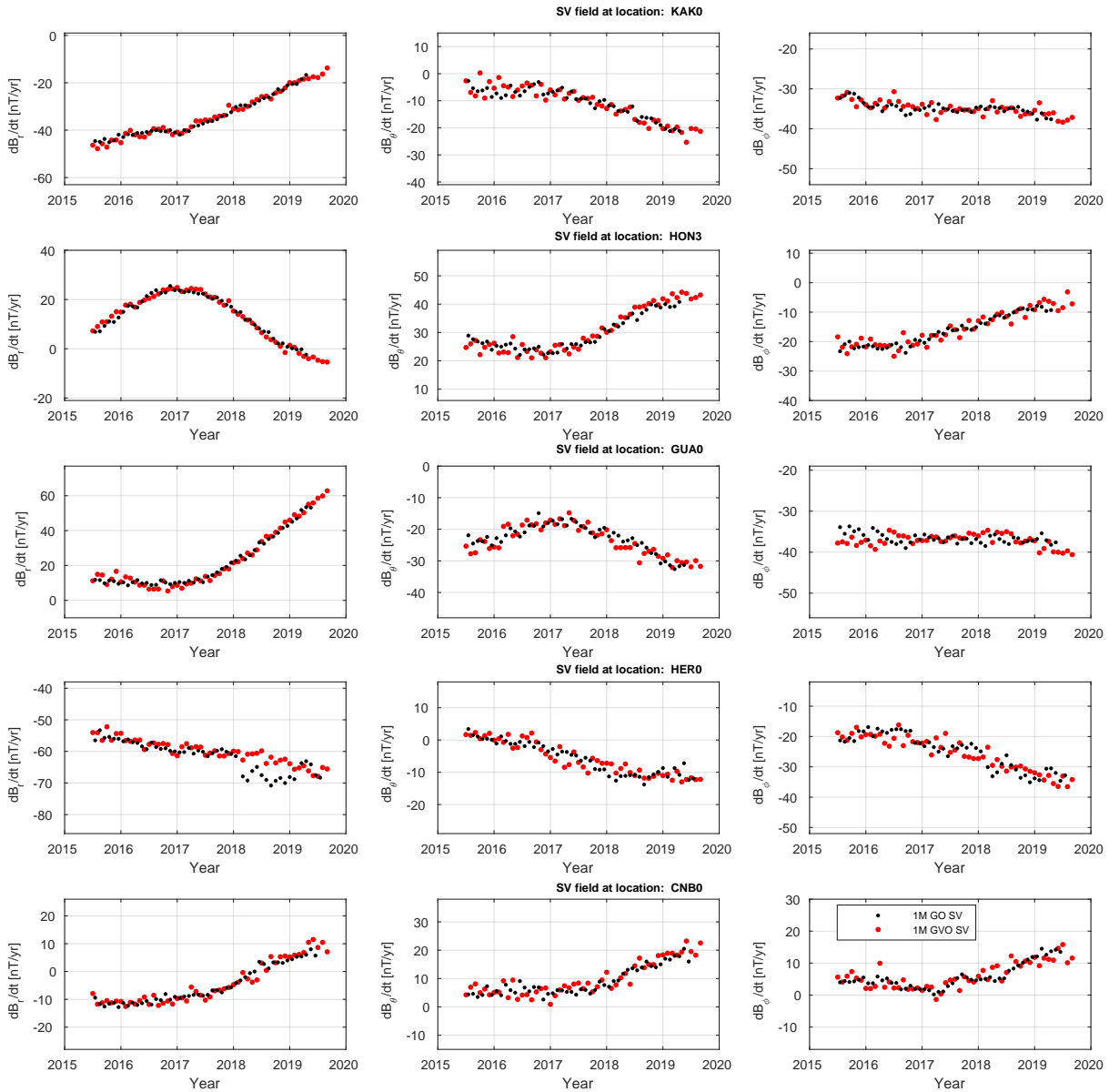
Figure 14: One-monthly Core Field GVO Secular Variation estimates (calculated using annual differences) mapped to Earth's surface (red symbols) and one-monthly revised monthly means from selected high quality 'benchmark' ground observatories from mid and low latitude (black symbols), arranged from north to south in the rows. Left column is the radial field component, middle column is the southward field component, right column is the eastward field component, units are nT.

The absolute levels (i.e. amplitude of secular variation) and trends (i.e. secular acceleration) in these best available records of the core field secular variation at ground observatories are well matched by the one-monthly Core Field Secular Variation series. Peaks (secular variation impulses/jerks) such as that in the radial field in Honolulu in 2017 are well captured and there is

no indication of loss of temporal resolution compared to the ground records. This indicates time-dependent secular variation down to time scales of 1 year (the annual difference filter used for computing the SV in both the Ground Observatory and GVO records here) is well captured in the *Swarm* Core Field Secular Variation GVO product. A discrepancy is seen in the radial field secular variation in 2018 for Hermanus observatory; given the series at other observatories agree well, and there is good agreement at this location at other times, this discrepancy is difficult to understand in terms of the *Swarm* data and its processing. It may therefore be an operational issue related to the observatory. The scatter is larger for the GVO series considering the southward θ components and there are indications of remaining noise with period close to one year in the eastward ϕ components.

Further comparison of the one-monthly Core Field Secular Variation GVOs at non-polar observatories are shown in Figure 15. Again the amplitudes and trends in the secular variation in the GVO series agree well with those found at the ground observatories, with slightly higher scatter seen in the horizontal components of the GVOs.

Figure 15 shows similar comparisons for a selection of the polar observatories. Here the scatter is larger in both the ground and GVO data but again the observed trends agree well. There is a discrepancy between the GVO and ground series SV in GDH2 in 2018.

Next we consider in Table 9 the comparison between the one-monthly Core Field Secular Variation GVO estimates and the predictions of the CHAOS-7.2 internal field model. The comparisons are reported in terms of global statistics for all 300 GVO and sub-divided into 78 polar and 222 non-polar GVOs, as well as benchmark GVOs below 30 degrees latitude. We find impressive agreement between the field model predictions and the GVO estimates, even at polar latitudes, with all components agreeing to within 2.2 nT/yr. This indicates that the GVO secular variation signal agrees well with that found in the CHAOS-7.2 field model.

Model series	rms_r [nT/yr]	rms_θ [nT/yr]	rms_ϕ [nT/yr]	rms_F [nT/yr]
All	1.60	1.64	1.48	1.69
Polar	2.19	1.95	2.50	2.20
Non-polar	1.40	1.53	1.12	1.51
Benchmark	1.40	1.63	1.14	1.56

Table 9: One-monthly Core Field Secular Variation GVOs versus field model predictions: rms differences for the spherical polar vector components and field intensity in nT/yr.
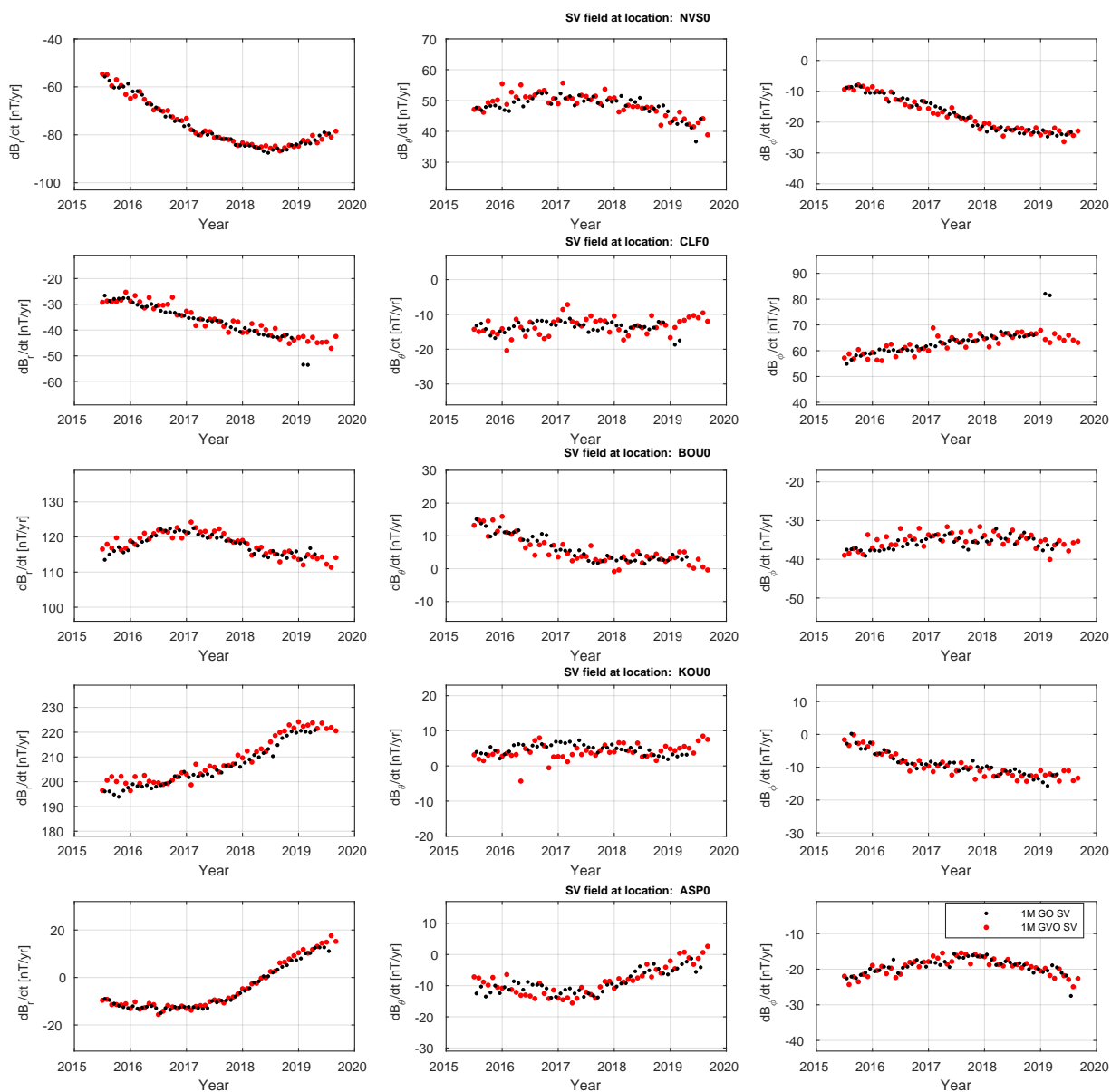
Figure 15: One-monthly Core Field GVO Secular Variation estimates (calculated using annual differences) mapped to Earth's surface (red symbols) and one-monthly revised monthly means from selected non-polar ground observatories (black symbols), arranged from north to south in the rows. Left column is the radial field component, middle column is the southward field component, right column is the eastward field component, units are nT.
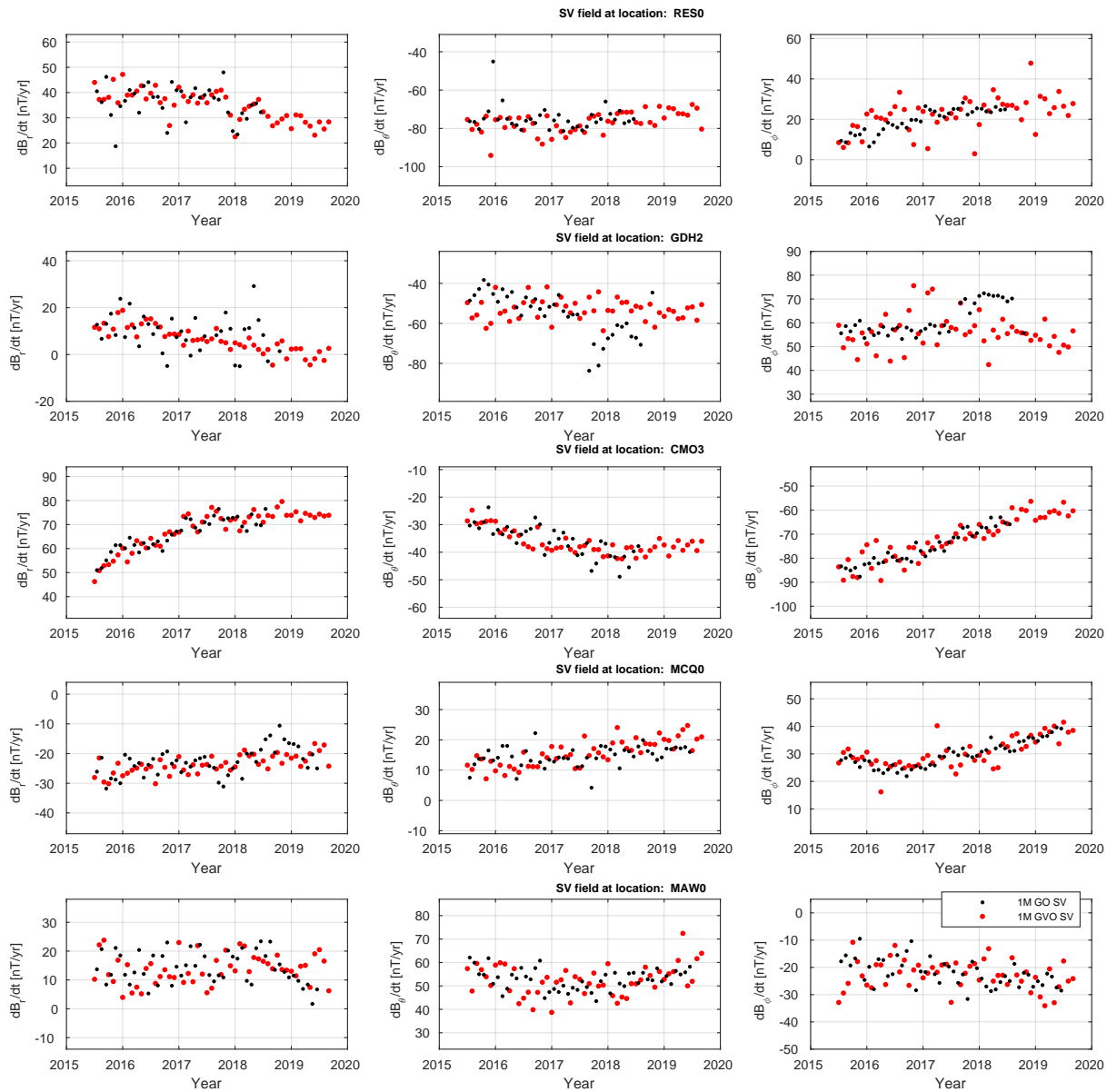
Figure 16: One-monthly Core Field GVO Secular Variation estimates (calculated using annual differences) mapped to Earth's surface (red symbols) and one-monthly revised monthly means from selected polar ground observatories (black symbols), arranged from north to south in the rows. Left column is the radial field component, middle column is the southward field component, right column is the eastward field component, units are nT.

3.2 Four-Monthly Core Field GVOs and Secular variation

Finally we consider validation tests for the four-monthly Core Field GVO product. This was computed using dark and quiet-time data selection, and with the removal of external and toroidal fields estimated epoch-by-epoch using spherical harmonic analysis. Comparisons with revised four-monthly mean Ground Observatory records and the secular variation predicted by the CHAOS-7.2 field model.

Table 10 presents the rms differences between the four-monthly revised means ground observatory time series and the 4-monthly GVO core field time series at each selected observatory location, mapped down to the Earth's surface. The averages rms values considering all considered stations are 2.18 nT, 3.19 nT and 2.52 nT for the radial, θ and ϕ components, respectively. The agreement at the benchmark observatories is below 2 nT in all components, and only 1.42 nT for the scalar field.

Observatory	rms_r^{obs} [nT]	$\mathrm{rms}_\theta^{obs}$ [nT]	rms_ϕ^{obs} [nT]	rms_F^{obs} [nT]
ABK	1.37	4.27	4.24	1.58
ASC	1.23	1.25	2.17	1.18
ASP	0.58	3.52	0.95	1.92
BOU	1.61	1.91	1.47	1.28
BRW	6.25	2.85	2.48	6.31
CLF	1.14	1.13	1.67	0.77
CMO	3.09	5.56	2.44	3.39
CNB	1.10	2.50	1.58	0.42
GAN	1.03	3.39	1.75	3.24
GDH	5.19	4.73	3.50	5.08
GUA	1.09	1.47	1.22	1.59
HER	1.16	1.47	2.17	1.43
HON	1.15	1.77	1.65	1.56
HRN	4.83	3.92	4.79	4.63
HUA	6.25	2.85	2.48	6.31
KAK	1.18	3.18	1.94	2.77
KOU	2.84	2.45	1.67	2.18
LRM	0.92	2.91	1.61	1.76
MAW	5.36	13.18	6.49	5.57
MBO	3.37	3.70	3.99	3.81
MCQ	1.64	1.82	1.55	1.20
NAQ	2.56	6.05	3.30	1.35
NGK	0.79	0.88	1.90	0.70
NSV	2.12	1.31	2.71	1.93
PST	1.48	2.76	1.67	1.01
RES	3.89	1.95	3.27	3.87
SHU	1.93	4.12	3.26	1.27
TDC	0.82	2.47	2.24	1.96
ALL	2.18	3.19	2.52	2.38
Polar	3.25	4.25	3.39	3.12
Non-Polar	1.26	2.28	1.76	1.74
Benchmark	1.14	1.92	1.70	1.42

Table 10: Four-monthly Core Field GVOs versus selected Ground Observatories: rms differences for the spherical polar vector components and field intensity in nT.

Table 11 presents statistics of the rms differences between the global grid of Core Field GVO products and the CHAOS-7.2 internal field model, after removal of the LCS-1 lithospheric model. Even in the polar regions the Core Field GVOs and the internal field model agree to within 3 nT. Best agreement is found for the eastward ϕ component at non-polar latitudes.

Model series	rms_r^{obs} [nT]	$\mathrm{rms}_\theta^{obs}$ [nT]	rms_ϕ^{obs} [nT]	rms_F^{obs} [nT]
All	2.51	2.34	2.06	2.51
Polar	2.96	3.36	2.96	2.87
Non-polar	2.35	1.98	1.74	2.38
Benchmark	2.39	2.03	1.73	2.50

Table 11: Four-monthly Core Field GVOs versus field model predictions: rms differences for the spherical polar vector components and field intensity in nT.

Statistics for the comparison of the secular variation recorded at ground observatories, obtained from annual differences of four-monthly revised mean values, and the Core Field Secular Variation GVO estimates (obtained from annual differences of the Core Field GVOs) are presented in Table 12.

Observatory	rms_r [nT/yr]	rms_θ [nT/yr]	rms_ϕ [nT/yr]	rms_F [nT/yr]
ABK	7.07	8.85	11.18	2.05
ASC	1.43	1.10	4.15	1.85
ASP	0.94	1.08	1.08	1.11
BOU	2.02	1.12	1.88	1.72
BRW	12.29	7.18	13.36	10.17
CLF	1.63	1.55	2.39	0.99
CMO	8.67	4.45	9.92	4.33
CNB	0.61	1.62	1.85	0.47
GAN	0.74	2.46	2.49	2.22
GDH	10.21	9.01	7.59	7.88
GUA	1.06	1.64	2.01	1.76
HER	2.40	1.06	2.73	2.17
HON	1.45	1.18	1.74	0.80
HRN	13.72	8.38	5.90	6.39
HUA	12.29	7.18	13.36	10.17
KAK	1.37	2.22	2.11	0.96
KOU	3.08	2.32	2.24	1.01
LRM	1.17	1.61	1.39	1.46
MAW	4.13	17.13	7.40	4.42
MBO	1.99	2.37	4.76	1.49
MCQ	2.15	2.63	2.10	2.15
NAQ	2.90	10.22	4.69	0.88
NGK	1.29	1.31	2.44	1.00
NSV	1.24	1.60	4.66	1.22
PST	2.32	4.88	2.20	1.61
RES	8.22	8.14	5.38	6.38
SHU	1.71	2.20	4.83	1.73
TDC	0.56	1.34	3.02	2.34
ALL	3.49	3.99	4.27	2.63
Polar	5.83	6.59	6.49	3.81
Non-Polar	1.47	1.73	2.34	1.60
Benchmark	1.42	1.54	2.14	1.19

Table 12: Four-monthly Core Field Secular Variation GVO versus selected Ground Observatories: rms differences for the spherical polar vector components and field intensity in nT/yr.

The average rms values considering all stations are $3.49\,\mathrm{nT/yr}$, $4.30\,\mathrm{nT/yr}$, $4.45\,\mathrm{nT/yr}$ for the radial, θ and ϕ components, respectively. The scalar field secular variation at the benchmark GVOs agrees to within 1.2 nT/yr and is for example only $0.5\,\mathrm{nT/yr}$ at the Canberra observatory (CNB) in Australia. Note that in computing these statistics only data from 2014 to 2018 was used, to avoid complications related to non-definitive data close to the end of the GVO series.

Figures 17-19 present plots of the four-monthly ground observatory SV (black dots) and four-monthly GVO SV (red dots).

In Figure 17 comparisons at five of the benchmark locations are shown. The scatter seen in the one-monthly Core Field Secular Variation time series is reduced and these independent

series illustrate the excellent agreement in the secular variation recorded in the four-monthly GVO series and that seen at ground observatories. The peak in the secular variation seen in the radial component at Honolulu (HON3) in 2017 is well captured as is the change in slope seen at Guam (GUA0) in mid-2017. Some small differences between the GVO series and the ground observatory series are seen in the eastward ϕ components especially in 2015 and 2016 when it is well known there was enhanced magnetospheric and ionospheric activity.
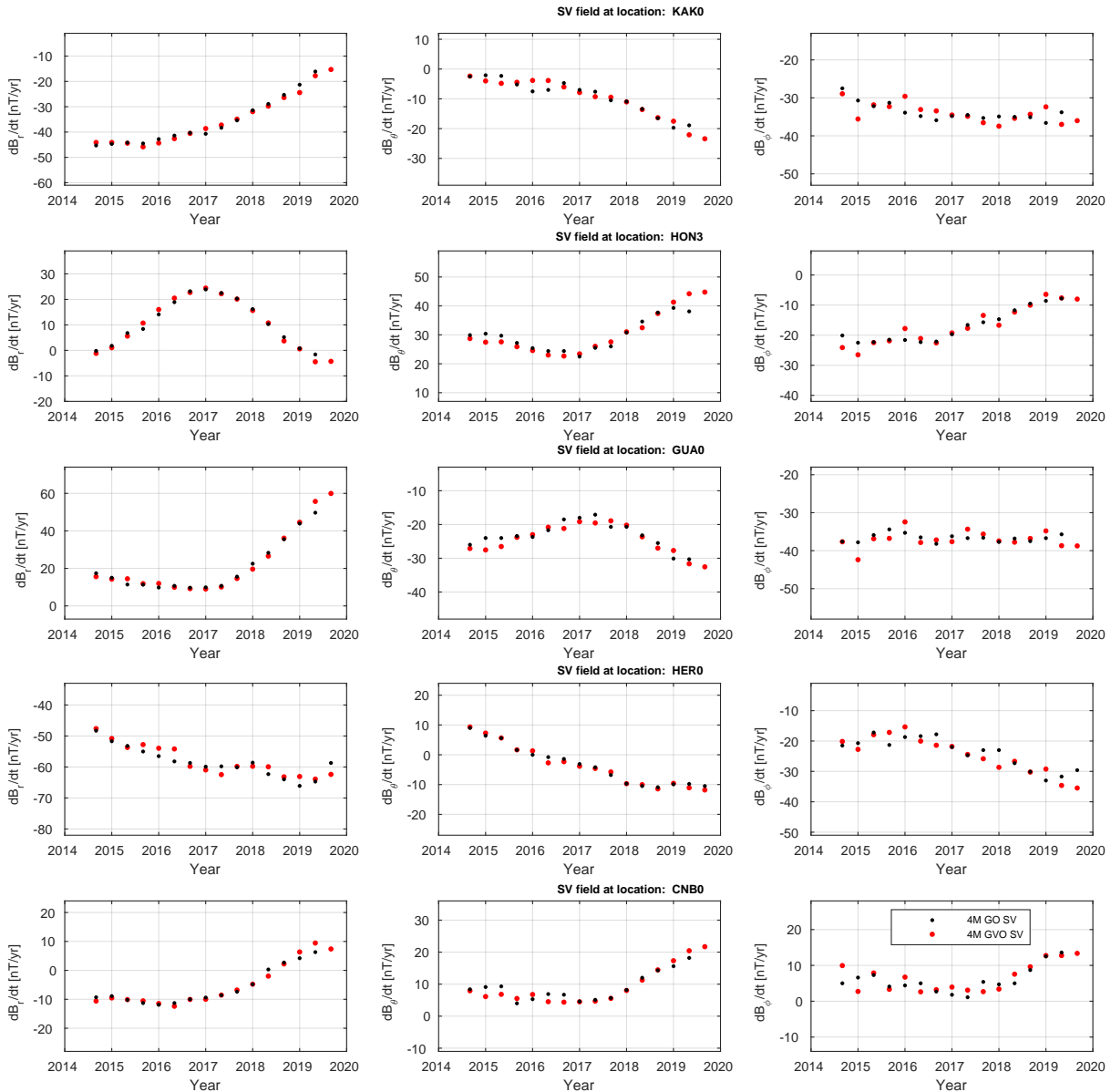
Figure 17: Four-monthly Core Field GVO Secular Variation estimates (calculated using annual differences) mapped to Earth's surface (red symbols) and four-monthly revised means from selected high quality 'benchmark' ground observatories from mid and low latitude (black symbols), arranged from north to south in the rows. Left column is the radial field component, middle column is the southward field component, right column is the eastward field component, units are nT.

Figure 18 shows further comparisons of the four-monthly secular variation at non-polar stations.

Again the results are encouraging with field accelerations being well captured, for example in Alice Springs (ASP0) in 2017. Larger disagreements are often seen in the final year of the series, when the ground observatory data is not yet definitive, and the RC index used in deriving the revised monthly means is less reliable. This is the reason we used only data up to 2018 when computing the rms statistics.
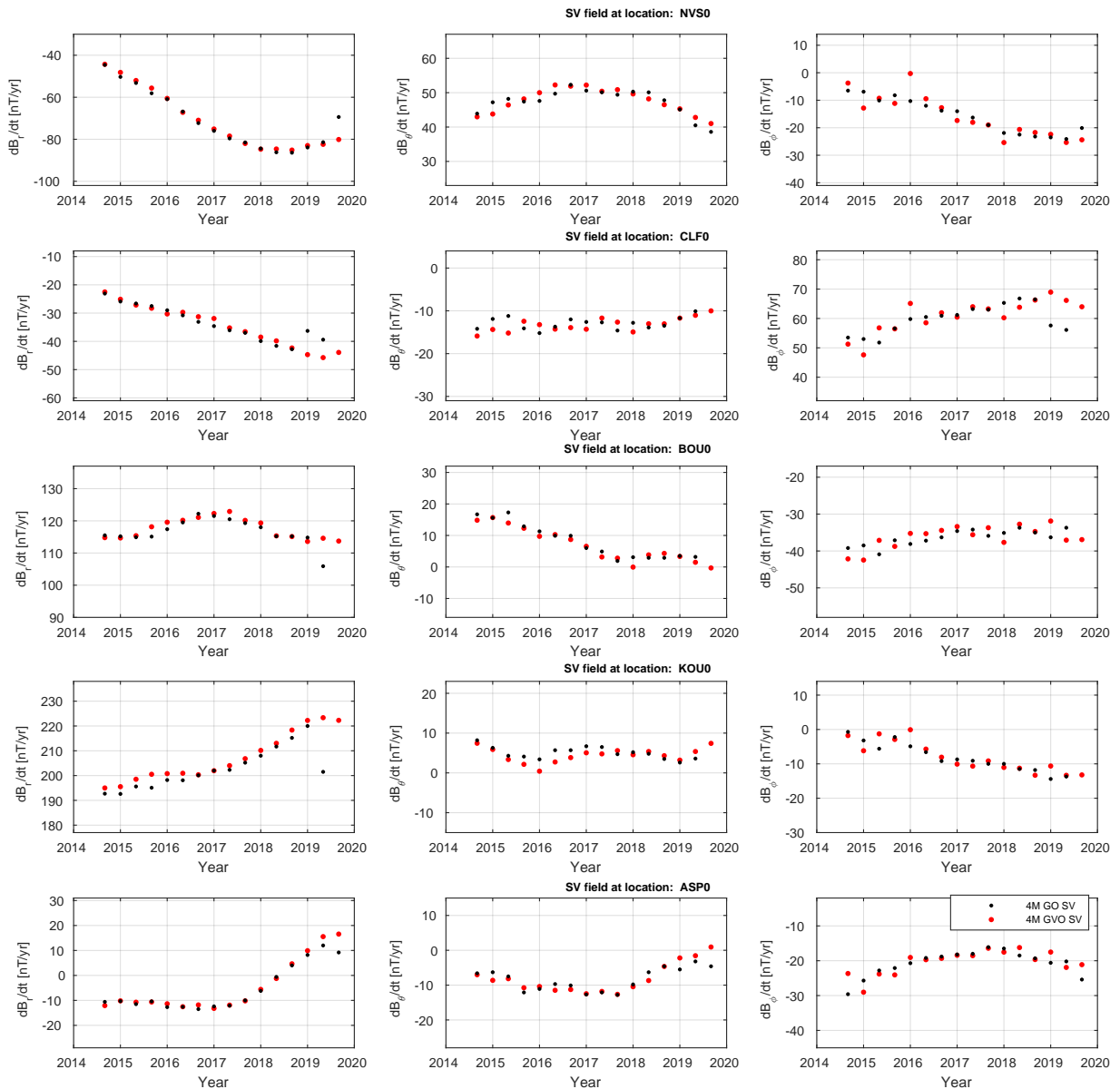
Figure 18: Four-monthly Core Field GVO Secular Variation estimates (calculated using annual differences) mapped to Earth's surface (red symbols) and four-monthly revised means from selected non-polar ground observatories from mid and low latitude (black symbols), arranged from north to south in the rows. Left column is the radial field component, middle column is the southward field component, right column is the eastward field component, units are nT.

Figure 19 presents example comparison of the four-monthly secular variation in the polar region. Despite the slightly higher scatter the agreement is again encouraging with trends seen in ground

stations being well captured at the GVO's e.g. at College Station (CMO3) in Alaska. Largest differences are seen for Mawson station (MAW) in Antarctica where a sawtooth pattern about the ground series is visible in the four-monthly GVO estimates. This enhanced scatter is reflected in the error estimates supplied together with the GVO products, but illustrates that caution is needed when interpreting SV variations on interannual and shorter timescales in the auroral zone. Further work is required to better understand these discrepancies.
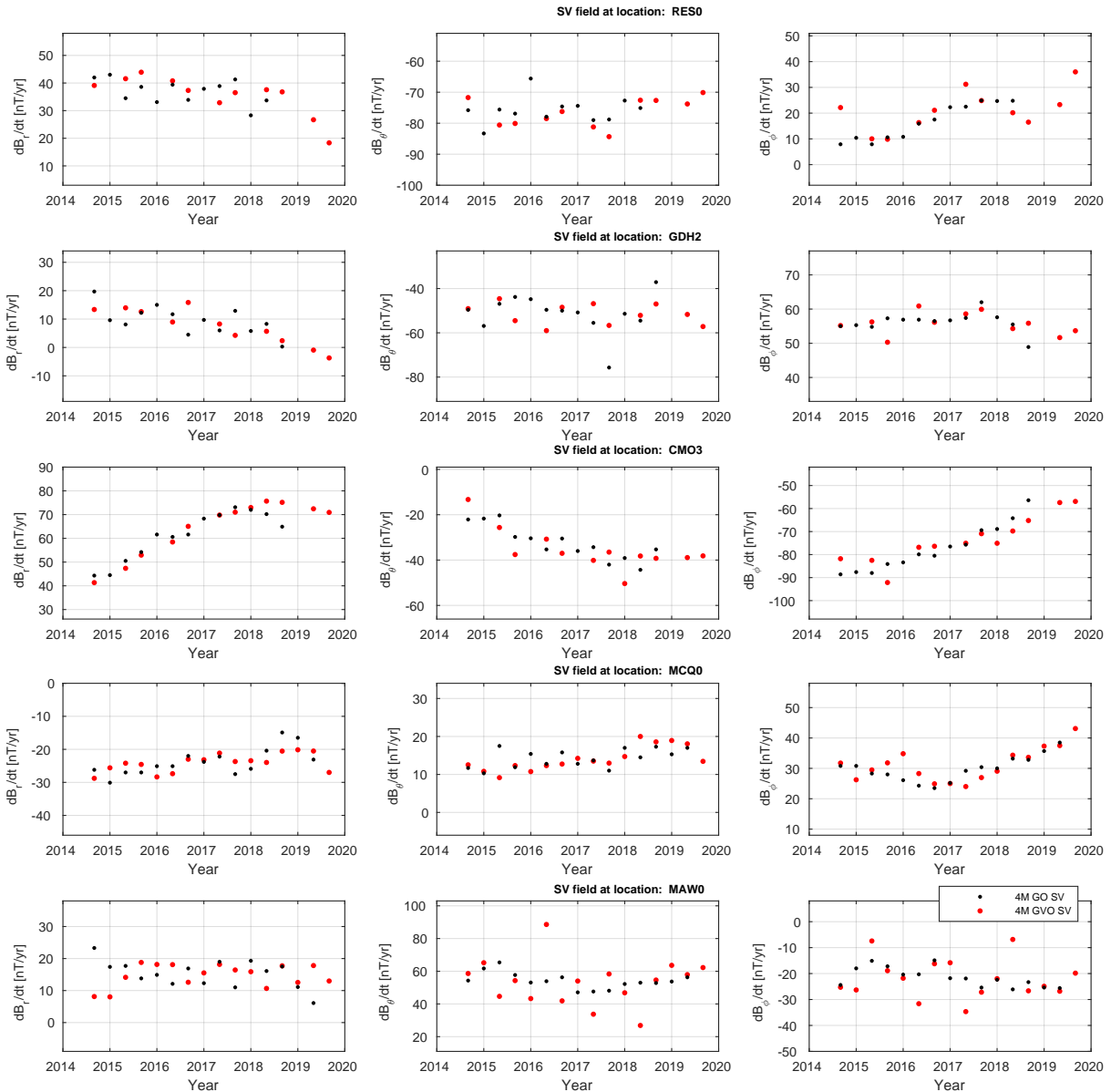
Figure 19: Four-monthly Core Field GVO Secular Variation estimates (calculated using annual differences) mapped to Earth's surface (red symbols) and four-monthly revised means from selected polar ground observatories (black symbols), arranged from north to south in the rows. Left column is the radial field component, middle column is the southward field component, right column is the eastward field component, units are nT.

Table 13 presents the rms differences between the secular variation predicted by the CHAOS-7.2 field model and the four-monthly GVO Core Field SV estimates. The reported rms differences for all components for all regions are below $3.4\,\mathrm{nT/yr}$, with differences of only $1\,\mathrm{nT/yr}$ for the non-Polar r and θ components and $2\,\mathrm{nT/yr}$ for the ϕ component. The rms difference between the benchmark GVOs below 30 degree latitude, and the CHAOS-7.2 field model is $0.97\,\mathrm{nT/yr}$ for the field intensity.

Model series	rms_r [nT/yr]	rms_θ [nT/yr]	rms_ϕ [nT/yr]	rms_F [nT/yr]
All	1.27	1.42	2.38	1.44
Polar	2.15	2.68	3.38	2.79
Non-polar	0.96	0.98	2.03	0.96
Benchmark	0.97	0.97	2.02	0.97

Table 13: Four-monthly Core Field Secular Variation GVOs versus field model predictions: rms differences for the spherical polar vector components and field intensity in nT/yr.

4 Summary

Here we summarize the statistical findings of this validation report in the form of two summary tables. Table 14 collects results of the validation tests against independent ground observatories and established global field models for the one-monthly GVO products, while Table 15 collects similar statistics for four-monthly GVOs. The error estimates provided along with the products are also presented in these tables for reference.

	Model series	Ground Obs Comparison				Model Comparison				Error Estimates		
		rms_r	rms_θ	rms_ϕ	rms_F	rms_r	rms_θ	rms_ϕ	rms_F	rms_r	rms_θ	rms_ϕ
All												
	Obs GVO [nT]	3.00	6.98	5.25	3.91	4.16	3.59	4.00	3.83	4.17	7.18	6.92
	Core GVO [nT]	4.12	5.17	3.55	4.37	3.84	2.83	2.16	3.67	3.42	2.78	1.85
	Core SV GVO [nT/yr]	3.06	4.35	3.60	3.18	1.60	1.64	1.48	1.69	1.62	1.66	1.32
Polar												
	Obs GVO [nT]	4.28	10.30	7.27	4.83	5.47	5.24	5.19	5.30	8.13	14.44	15.71
	Core GVO [nT]	5.35	7.42	5.26	5.35	4.25	3.51	2.92	4.25	4.00	3.58	2.76
	Core SV GVO [nT/yr]	4.46	6.11	5.03	4.25	2.19	1.95	2.50	2.20	2.22	1.96	1.87
Non-polar												
	Obs GVO [nT]	1.90	4.11	3.51	3.12	3.70	3.01	3.59	3.31	2.78	4.63	3.83
	Core GVO [nT]	3.05	3.23	2.08	3.52	3.69	2.59	1.89	3.46	3.22	2.50	1.53
	Core SV GVO [nT/yr]	1.86	2.83	2.35	2.26	1.40	1.53	1.12	1.51	1.41	1.55	1.13
Benchmark												
	Obs GVO [nT]	1.67	3.71	3.32	2.53	3.80	3.10	3.66	3.42	3.92	4.69	4.36
	Core GVO [nT]	2.81	2.45	2.22	2.80	3.80	2.75	1.89	3.58	3.30	2.66	1.55
	Core SV GVO [nT/yr]	1.80	2.50	2.35	**1.75**	1.40	1.63	1.14	**1.56**	1.42	1.64	1.15

Table 14: Summary of validation tests for the one-monthly GVO products.

	Model series	Ground Obs Comparison				Model Comparison				Error Estimates		
		rms_r	rms_θ	rms_ϕ	rms_F	rms_r	rms_θ	rms_ϕ	rms_F	rms_r	rms_θ	rms_ϕ
All												
	Obs GVO [nT]	2.28	3.72	2.69	2.66	2.35	2.66	2.03	2.56	1.77	3.35	2.77
	Core GVO [nT]	2.18	3.19	2.52	2.38	2.51	2.34	2.06	2.51	2.28	2.20	1.88
	Core SV GVO [nT/yr]	3.49	3.99	4.27	2.63	1.27	1.42	2.38	1.44	1.31	1.47	2.29
Polar												
	Obs GVO [nT]	3.16	4.50	3.29	3.07	2.69	3.78	3.27	2.55	3.16	5.83	6.13
	Core GVO [nT]	3.25	4.25	3.39	3.12	2.96	3.36	2.96	2.87	2.65	3.29	2.78
	Core SV GVO [nT/yr]	5.83	6.59	6.49	3.81	2.15	2.68	3.38	2.79	2.23	2.78	2.84
Non-polar												
	Obs GVO [nT]	1.51	3.04	2.17	2.31	2.23	2.26	1.59	2.56	1.32	2.54	1.67
	Core GVO [nT]	1.26	2.28	1.76	1.74	2.35	1.98	1.74	2.38	2.16	1.82	1.56
	Core SV GVO [nT]	1.47	1.73	2.34	1.60	0.96	0.98	2.03	0.96	0.99	1.01	2.10
Benchmark												
	Obs GVO [nT]	1.32	2.92	1.93	1.93	2.26	2.41	1.56	2.74	1.28	2.16	1.30
	Core GVO [nT]	1.14	1.92	1.70	1.42	2.39	2.03	1.73	2.50	2.17	1.85	1.57
	Core SV GVO [nT/yr]	1.42	1.54	2.14	**1.19**	0.97	0.97	2.02	**0.97**	1.00	1.00	2.09

Table 15: Summary of validation tests for the four-monthly GVO products.

We find that both the one-monthly and four -monthly *Swarm* GVO products match independent ground observatory and field model predictions to within 5 nT in all components at non-polar latitudes. Given that the requirement for a good standard (Intermagnet) ground observatory is an accuracy of 5 nT, this indicates that the GVO method yields results comparable with good ground observatories. The four-monthly estimates agree even better, to within 3 nT.

Larger differences are found at polar latitudes where comparisons are complicated by the presence of strong ionospheric and magnetosphere-ionosphere coupling currents that are seen differently at ground and satellite altitude.

The processing applied to obtain core field GVOs results in even closer agreement with ground

observatory revised monthly means and with internal field models. Taking annual differences to obtain secular variation estimates further improves the agreement.

We find the secular variation of the field intensity in the one-monthly Core Field GVOs agrees with six benchmark ground observatories from mid and low latitudes to a level of 1.8 nT/yr. For the Four-monthly GVOs the difference drops to 1.2 nT/yr. These numbers may be considered an upper bound on the accuracy of the *Swarm* GVO secular variation estimates, since they also include the operational errors inherent in the ground observatories (perhaps 0.5 nT/yr at excellent observatories) as well as differences due to incomplete separation of non-core sources which will affect ground and GVO data in different ways.

We conclude that the GVO products developed during this project provide consistent and accurate global information on geomagnetic secular variation. We recommend the Core Field GVOs along with their supplied error estimates for use in studies of core dynamics. The Observed Field GVOs can also be used to study long period external field variations. Both applications will become increasingly attractive as the time series provided by the *Swarm* satellites lengthens.

Appendix

One-monthly Observed Field GVO comparisons
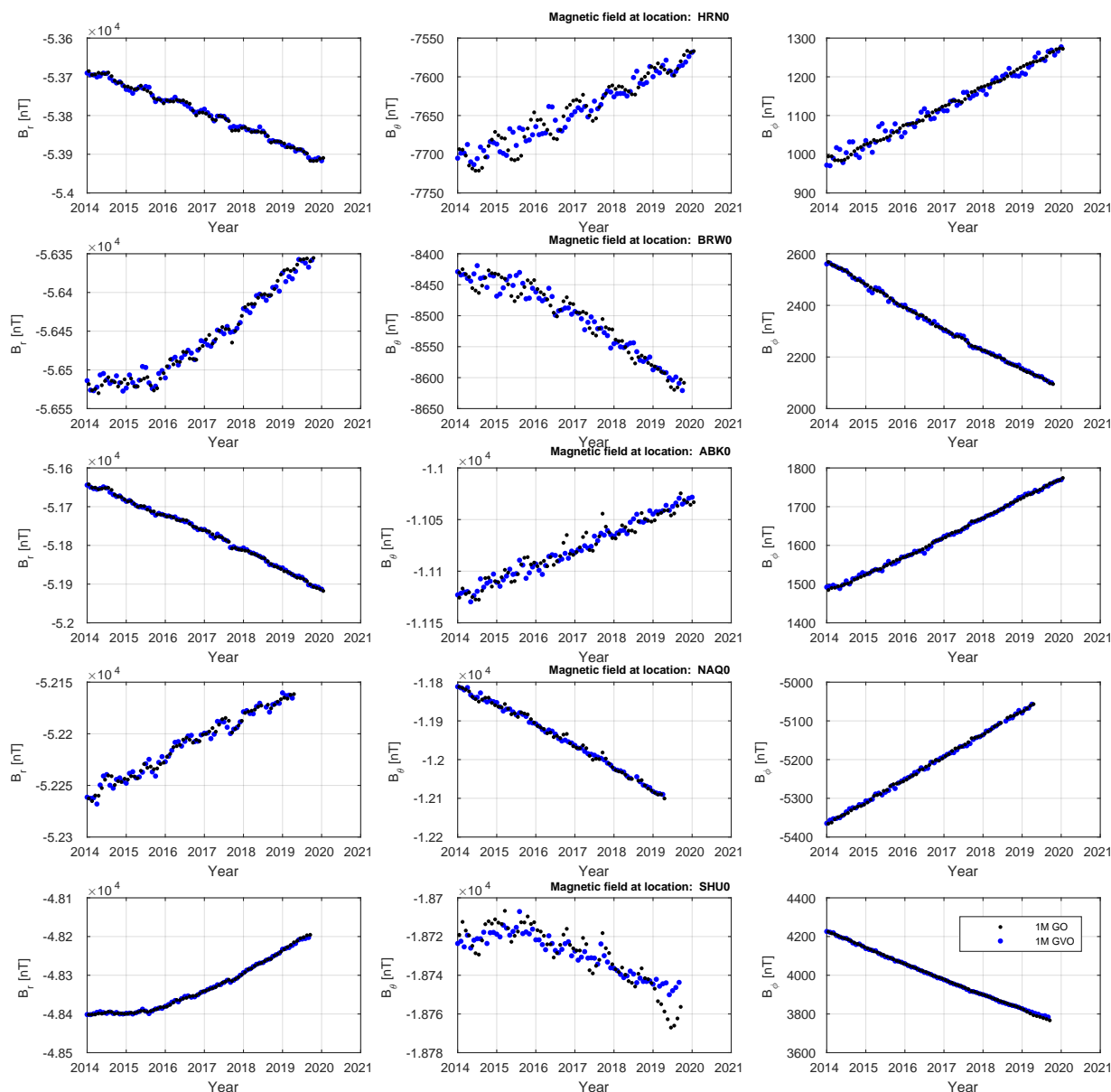
Figure 20: One-monthly Observed Field GVO estimates mapped to Earth's surface (blue symbols) and one-monthly means from selected ground observatories (black symbols), arranged from north to south in the rows. Left column is the radial field component, middle column is the southward field component, right column is the eastward field component, units are nT.
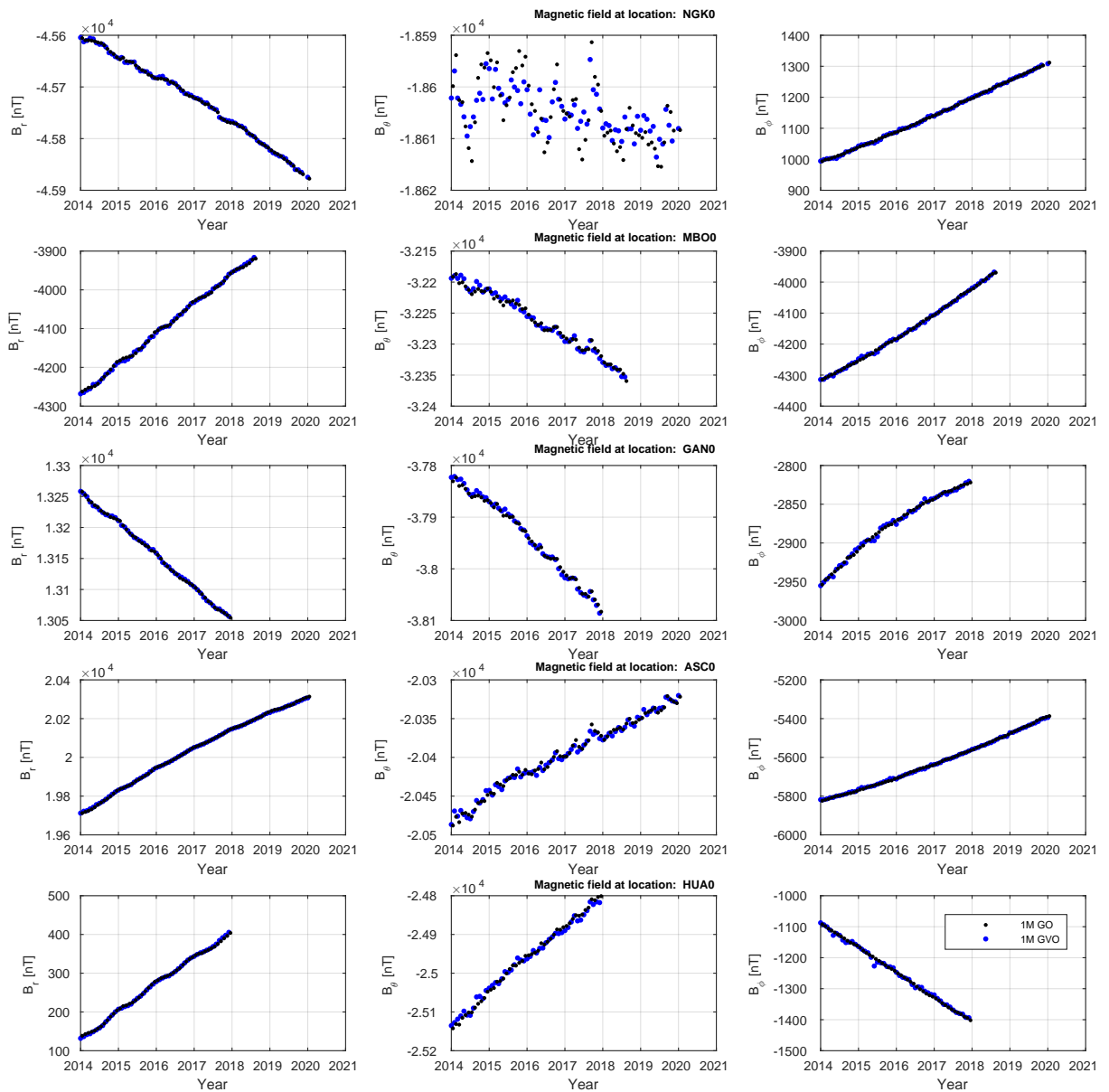
Figure 21: One-monthly Observed Field GVO estimates mapped to Earth's surface (blue symbols) and one-monthly means from selected ground observatories (black symbols), arranged from north to south in the rows. Left column is the radial field component, middle column is the southward field component, right column is the eastward field component, units are nT.
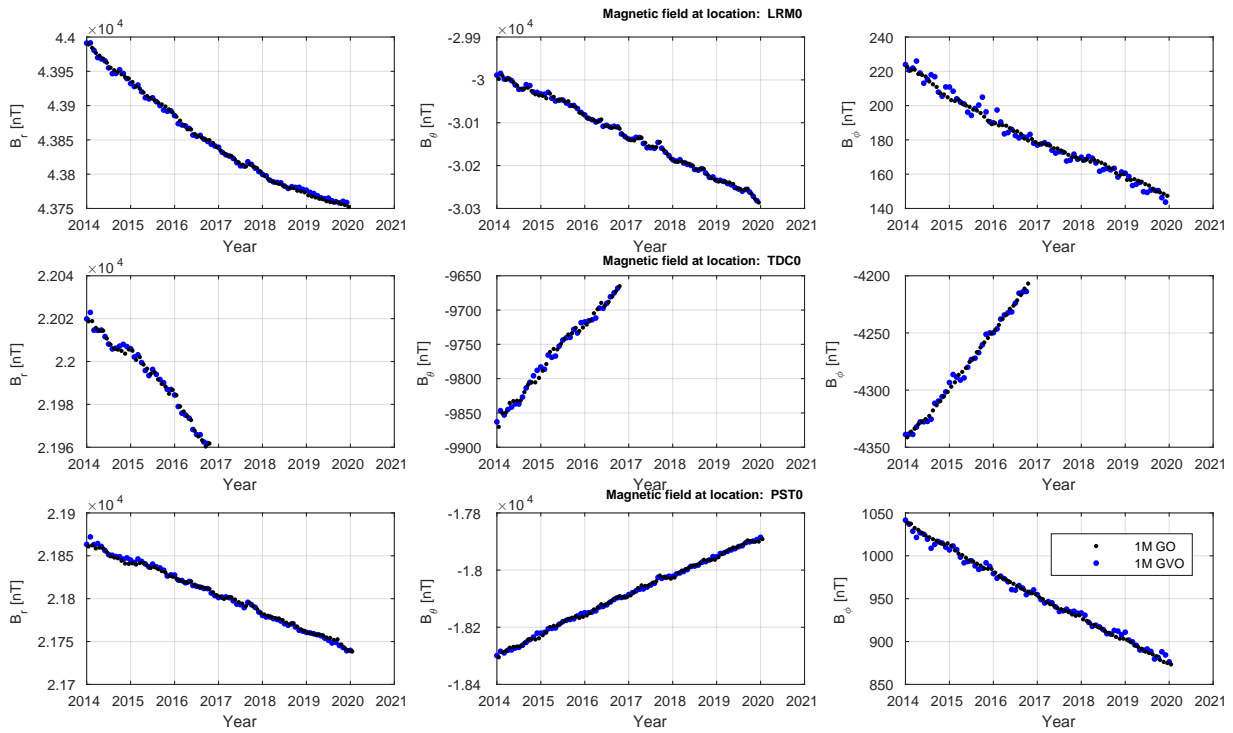
Figure 22: One-monthly Observed Field GVO estimates mapped to Earth's surface (blue symbols) and one-monthly means from selected ground observatories (black symbols), arranged from north to south in the rows. Left column is the radial field component, middle column is the southward field component, right column is the eastward field component, units are nT.

Four-monthly Observed Field GVO comparisons
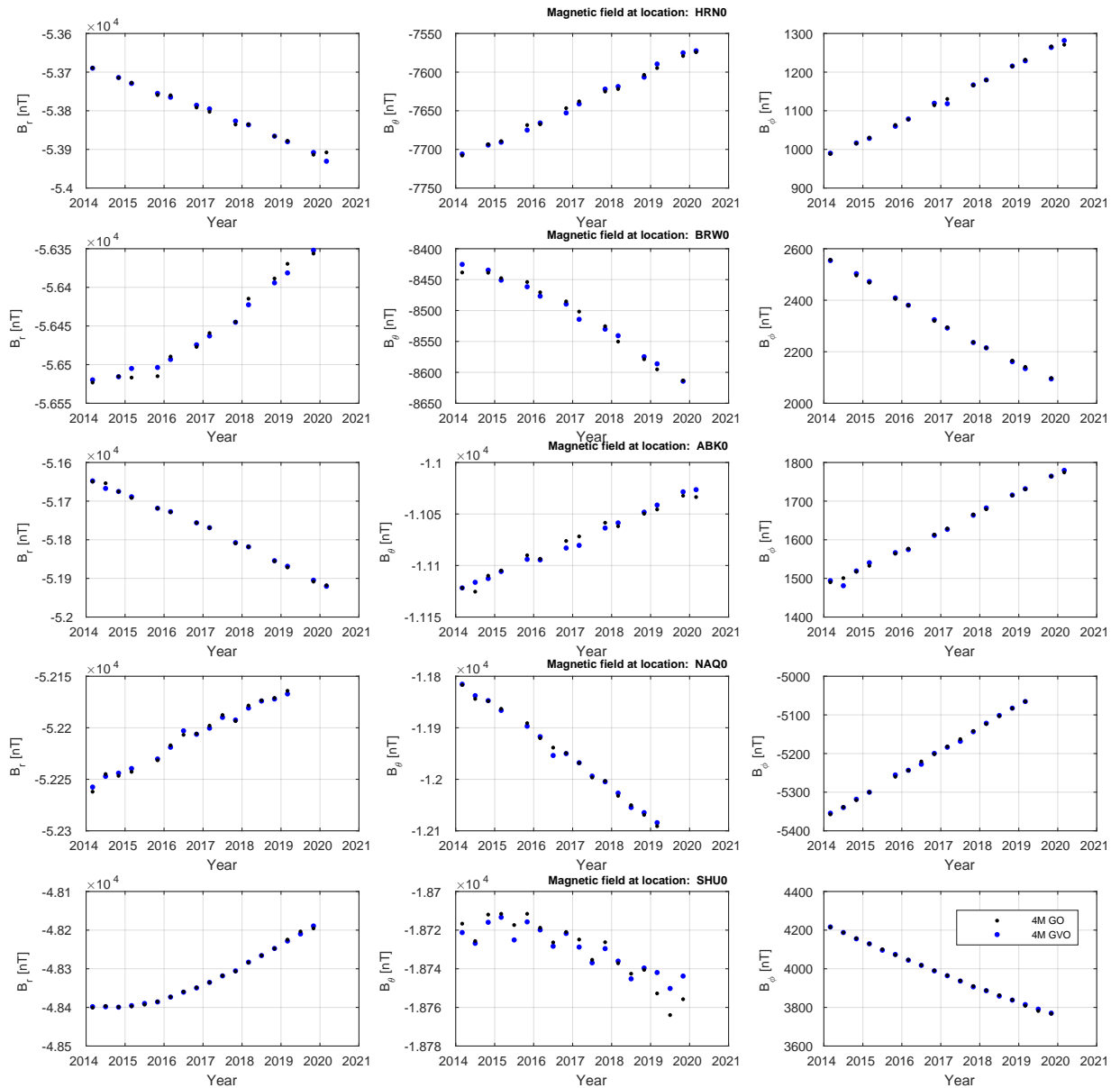
Figure 23: Four-monthly Observed Field GVO estimates mapped to Earth's surface (blue symbols) and four-monthly means from selected ground observatories (black symbols), arranged from north to south in the rows. Left column is the radial field component, middle column is the southward field component, right column is the eastward field component, units are nT.
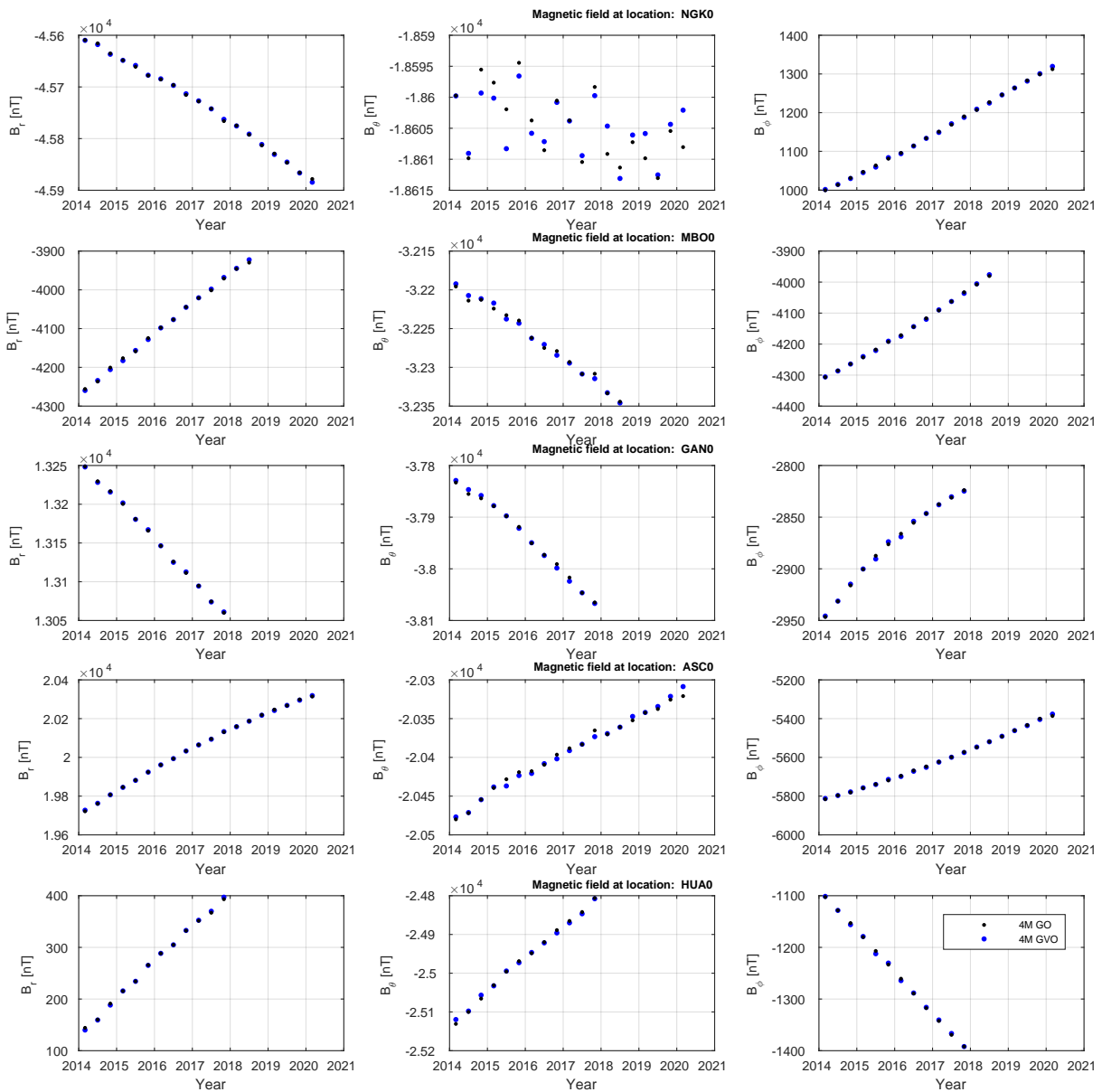
Figure 24: Four-monthly Observed Field GVO estimates mapped to Earth's surface (blue symbols) and four-monthly means from selected ground observatories (black symbols), arranged from north to south in the rows. Left column is the radial field component, middle column is the southward field component, right column is the eastward field component, units are nT.
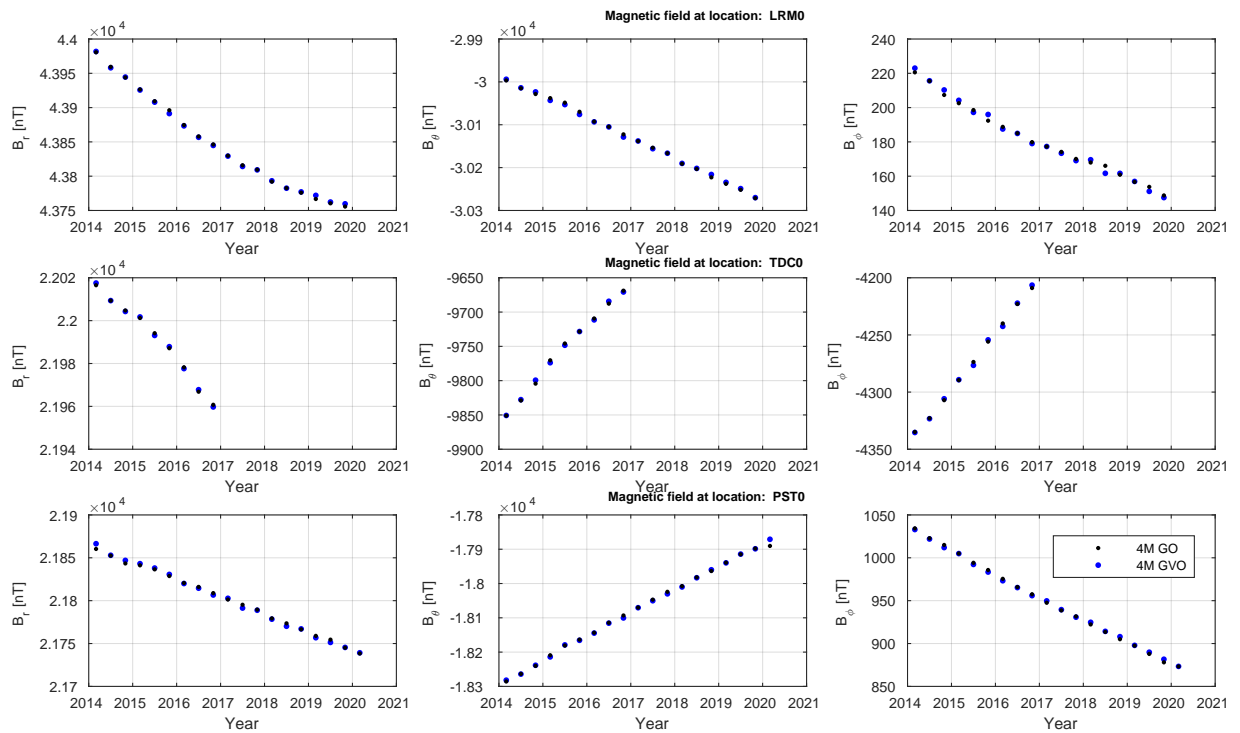
Figure 25: Four-monthly Observed Field GVO estimates mapped to Earth's surface (blue symbols) and four-monthly means from selected ground observatories (black symbols), arranged from north to south in the rows. Left column is the radial field component, middle column is the southward field component, right column is the eastward field component, units are nT.

One-monthly Core Field Secular Variation GVO comparisons
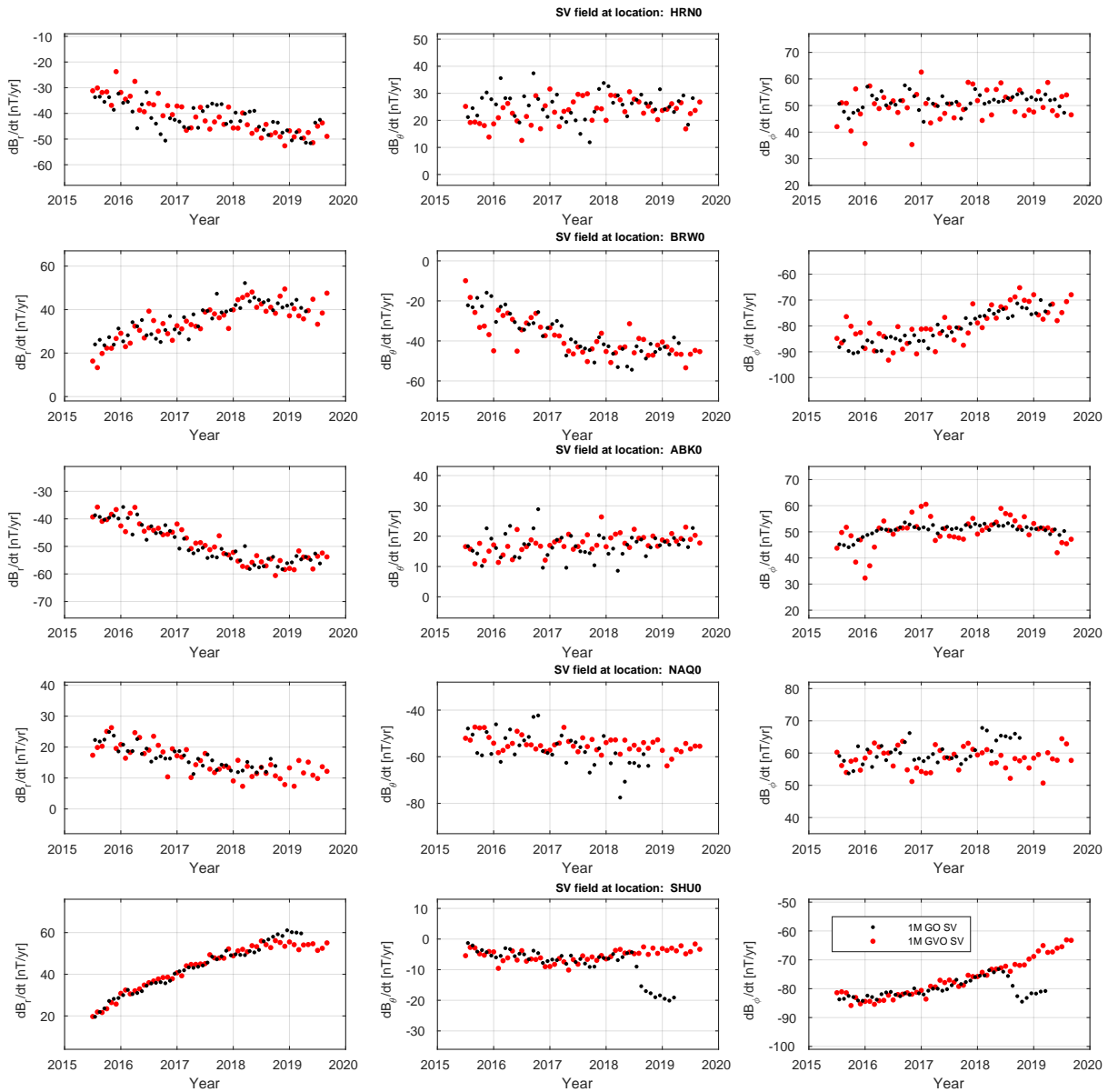
Figure 26: One-monthly Core Field GVO Secular Variation estimates (calculated using annual differences) mapped to Earth's surface (red symbols) and one-monthly revised means from selected ground observatories (black symbols), arranged from north to south in the rows. Left column is the radial field component, middle column is the southward field component, right column is the eastward field component, units are nT/yr.
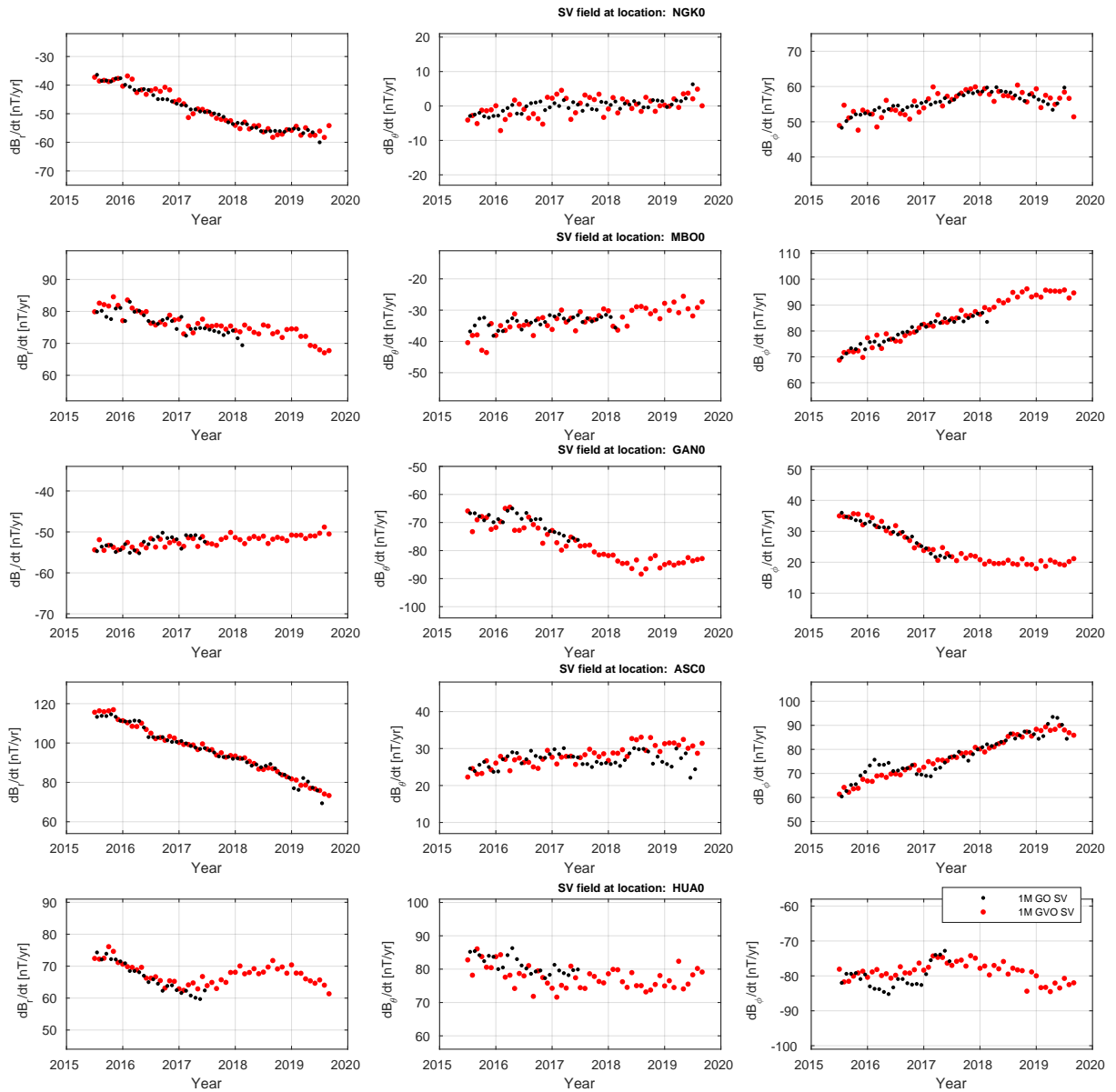
Figure 27: One-monthly Core Field GVO Secular Variation estimates (calculated using annual differences) mapped to Earth's surface (red symbols) and one-monthly revised means from selected ground observatories (black symbols), arranged from north to south in the rows. Left column is the radial field component, middle column is the southward field component, right column is the eastward field component, units are nT/yr.
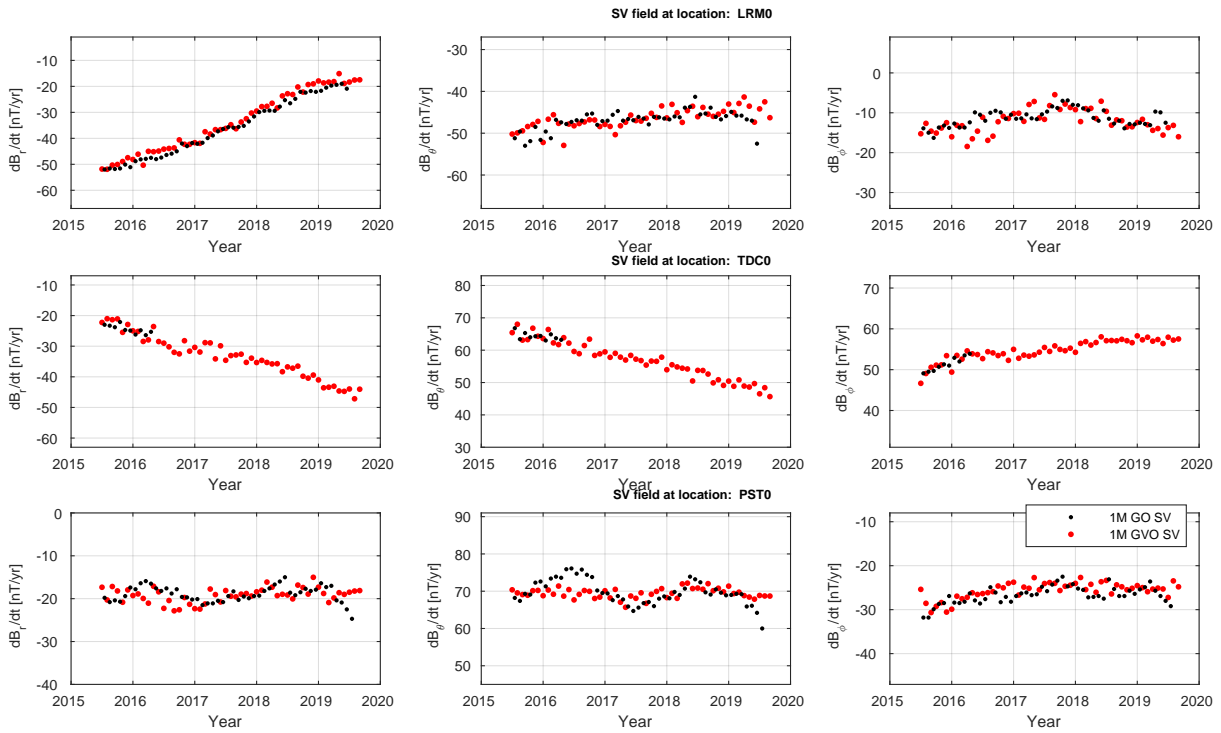
Figure 28: One-monthly Core Field GVO Secular Variation estimates (calculated using annual differences) mapped to Earth's surface (red symbols) and one-monthly revised means from selected ground observatories (black symbols), arranged from north to south in the rows. Left column is the radial field component, middle column is the southward field component, right column is the eastward field component, units are nT/yr.

Four-monthly Core Field Secular Variation GVO comparisons
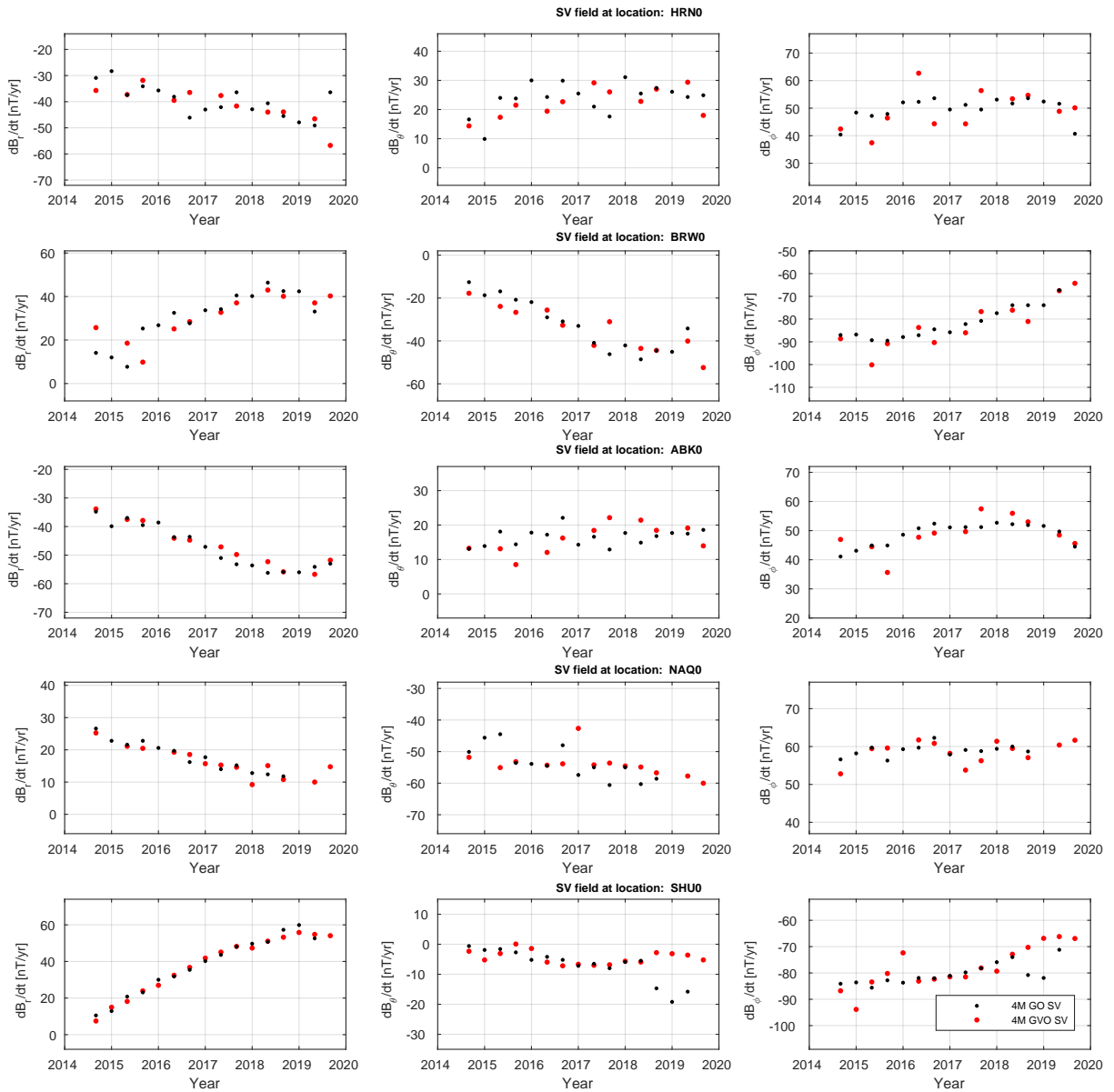
Figure 29: Four-monthly Core Field GVO Secular Variation estimates (calculated using annual differences) mapped to Earth's surface (red symbols) and four-monthly revised means from selected ground observatories (black symbols), arranged from north to south in the rows. Left column is the radial field component, middle column is the southward field component, right column is the eastward field component, units are nT/yr.
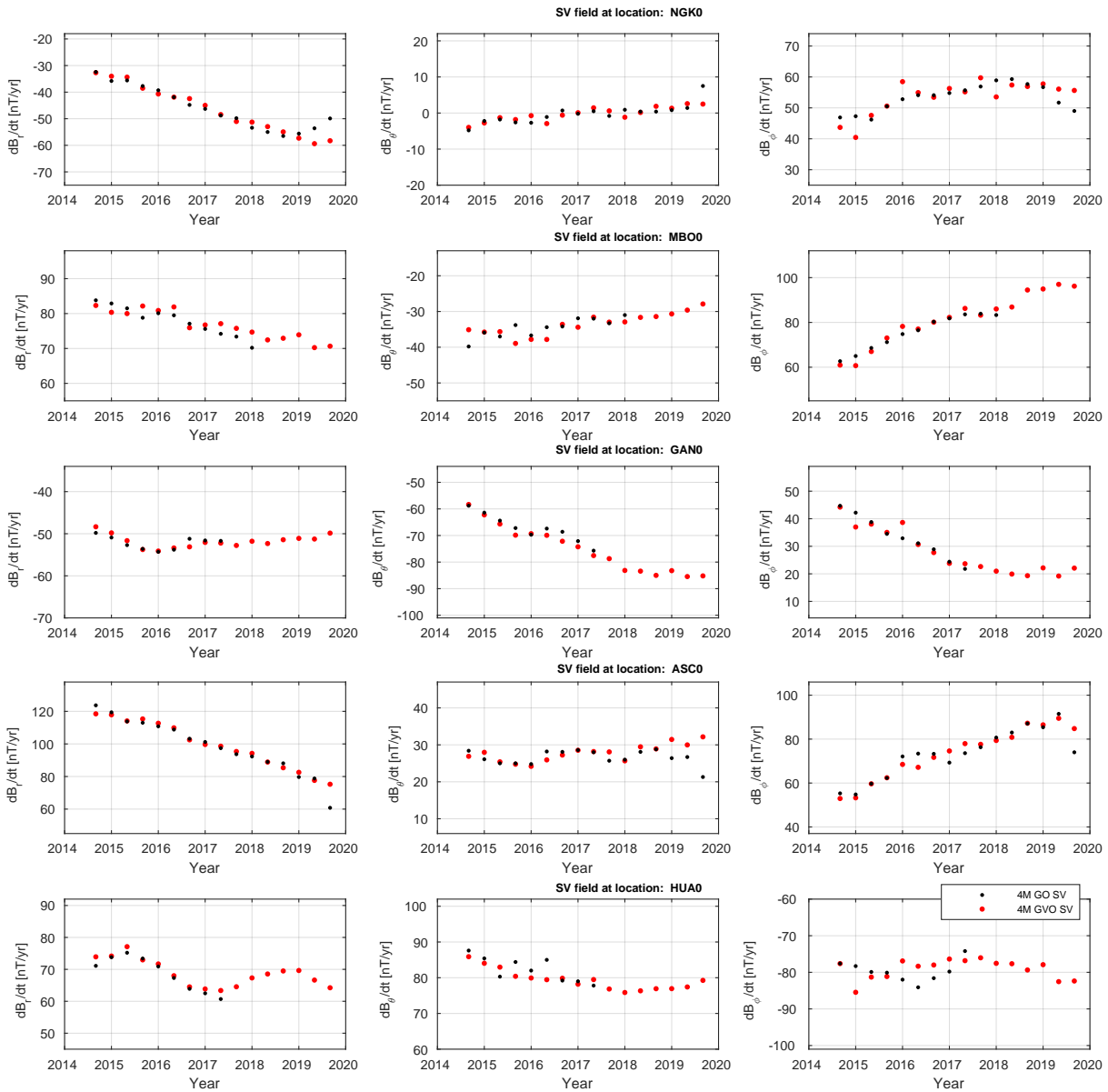
Figure 30: Four-monthly Core Field GVO Secular Variation estimates (calculated using annual differences) mapped to Earth's surface (red symbols) and four-monthly revised means from selected ground observatories (black symbols), arranged from north to south in the rows. Left column is the radial field component, middle column is the southward field component, right column is the eastward field component, units are nT/yr.
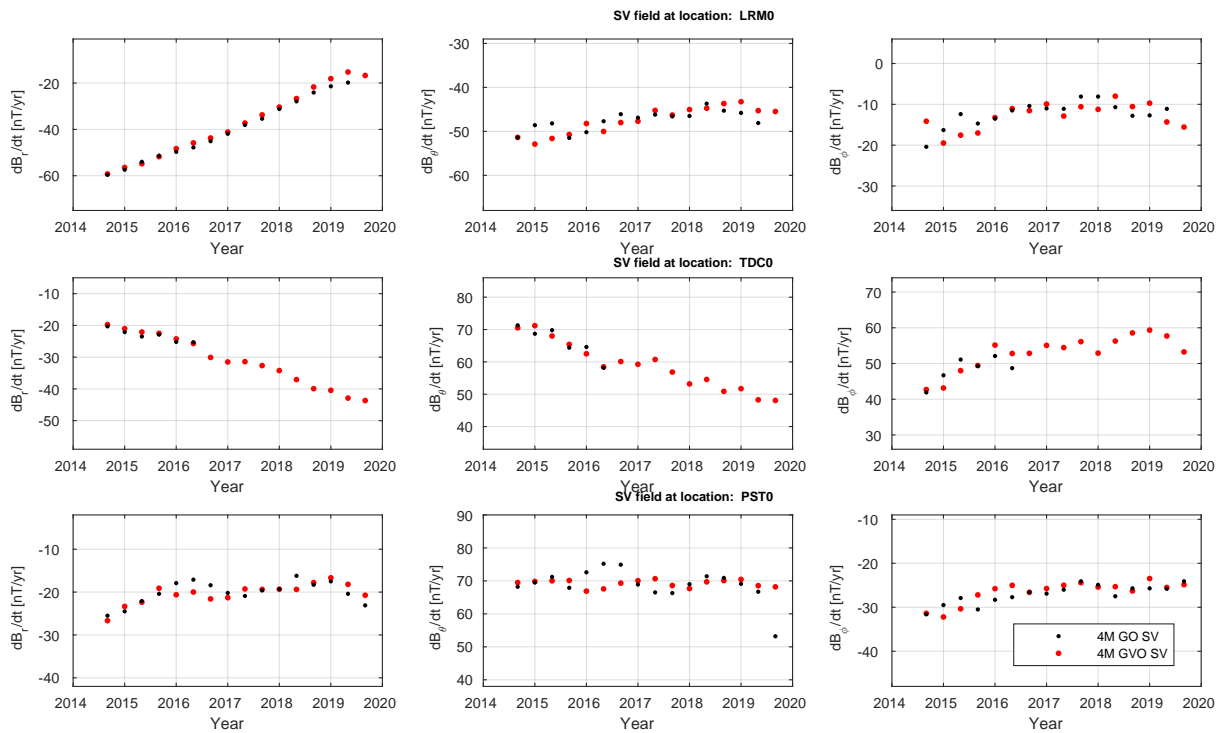
Figure 31: Four-monthly Core Field GVO Secular Variation estimates (calculated using annual differences) mapped to Earth's surface (red symbols) and four-monthly revised means from selected ground observatories (black symbols), arranged from north to south in the rows. Left column is the radial field component, middle column is the southward field component, right column is the eastward field component, units are nT/yr.

References

C. C. Finlay, C. Kloss, N. Olsen, M. Hammer, L. Tøffner-Clausen, A. Grayver, and A. Kuvshinov. The CHAOS-7 geomagnetic field model and observed changes in the South Atlantic Anomaly. *Earth, Planets and Space*, page (under review, 2020.

V. Lesur, B. Heumez, A. Telali, X. Lalanne, and A. Soloviev. Estimating error statistics for Chambon-la-Forêt observatory definitive data. *Annales Geophysicae*, 35(4):939–952, 2017. doi: 10.5194/angeo-35-939-2017.

S. Macmillan and N. Olsen. Observatory data and the Swarm mission. *Earth, Planets and Space*, 65:1355–1362, 2013.

N. Olsen, H. Lühr, C. C. Finlay, T. J. Sabaka, I. Michaelis, J. Rauberg, and L. Tøffner-Clausen. The CHAOS-4 geomagnetic field model. *Geophysical Journal International*, 197(2):815–827, 2014.

N. Olsen, D. Ravat, C. C. Finlay, and L. K. Kother. LCS-1: a high-resolution global model of the lithospheric magnetic field derived from CHAMP and Swarm satellite observations. *Geophysical Journal International*, 211(3):1461–1477, 2017.

T. J. Sabaka, L. Tøffner-Clausen, N. Olsen, and C. C. B. B. Finlay. A Comprehensive Model of the Earth's Magnetic Field Determined From 4 Years of Swarm Satellite Observations. *Earth, Planets and Space*, 2018. in Press.